ORTHOGONAL CHIRP DIVISION MULTIPLEXING TO IMPROVE RELIABILITY OF UNDERWATER ACOUSTIC COMMUNICATION

by

Cole Ferguson

Submitted in partial fulfillment of the requirements
for the degree of Master of Applied Science

at

Dalhousie University
Halifax, Nova Scotia
April 2023

This thesis is dedicated to everyone who had to suffer through the COVID-19 pandemic.

Table of Contents

List of Tables

List of Figures

Abstract

Covert underwater communication methods are constantly evolving, and there is a need for more robust techniques. In this thesis, the benefits and detriments of a number of currently in-use single-carrier covert underwater wireless acoustic communication techniques are described, with special attention paid to the chirp method for its robustness underwater. Multiple-carrier orthogonal frequency division multiplexing (OFDM) is then described as a way to improve bandwidth of underwater communications, and orthogonal chirp division multiplexing (OCDM) is investigated to determine if it can take advantage of the robustness of chirps and the throughput of OFDM. A comparison in simulation is made between OFDM and OCDM using channel data from St. Margaret's Bay in Halifax, Nova Scotia. The impact of the front end transmitter on the signal is investigated. An experiment is then performed in the Dalhousie Aquatron comparing OFDM and OCDM, and the results are discussed.

List of Abbreviations and Symbols Used

BER Bit Error Ratio.

CP Cyclic Prefix.

DBPSK Differential Binary Phase Shift Keying.

DFnT Discrete Fresnel Transform.

DFT Discrete Fourier Transform.

DSSS Direct-Sequence Spread-Spectrum.

FFT Fast Fourier Transform.

FH Frequency Hopping.

FH-BFSK Frequency Hopped Binary Frequency Shift Keying.

FHSS Frequency-Hopping Spread-Spectrum.

FSK Frequency Shift Keying.

ICI Inter-Carrier Interference.

IDFT Inverse Discrete Fourier Transform.

IFFT Inverse Fast Fourier Transform.

JANUS NATO standard for UWAC communication.

LFM Linear Frequency Modulation.

LPD Low Probability of Detection.

LPI Low Probability of Interception.

NATO North Atlantic Treaty Organization.

OCDM Orthogonal Chirp Division Multiplexing.

OFDM Orthogonal Frequency Division Multiplexing.

PN Pseudo-noise.

PRN Pseudo-Random Noise.

PSK Phase Shift Keying.

QAM Quadrature Amplitude Modulation.

TVR Transmit Voltage Response.

UWAC Underwater Acoustic Communication.

Acknowledgements

Thank you to Dr. Jean-François Bousquet for the enormous amount of support and guidance he provided while I was completing this research. This thesis would not have been possible without him.

Thank you to my girlfriend Cait, and to my parents David and Janice, and to my many friends for always supporting me and believing in me.

And thank you to Surinder, Ningcheng, Hossein, Jeff, and Adam for making the research work fun while I was at Dalhousie.

Chapter 1

Introduction

1.1 Background

The global average temperature of Earth has been rising annually, with no sign of stopping in the future [1]. One major impact of these rising temperatures is melting sea ice. Every year, Arctic sea ice melts and freezes with the seasons. In September 2020, Arctic sea ice nearly reached record lows, declining to the second lowest amount on record for the month of September [2]. Assuming that the global warming trend continues, difficult-to-access waterways in the northern regions of Canada, including the Northwest Passage, will be clear for ocean vessels for longer periods of time each year. This could result in increased shipping activity in the Arctic Ocean for trade, oil & gas exploration, research, and necessarily defence. There have always been debates over what constitutes "Canadian" territory in the Arctic: the Northwest Passage in particular is disputed by multiple countries [3]. A more accessible Northwest Passage would create a shorter route for North American ships to connect the Pacific and Atlantic oceans and would reduce the need for ships to travel south toward the Panama Canal. Canada and its ports stand to benefit greatly from increased traffic in the area if it is considered Canadian waters. These debates over territory will only become more serious as the planet warms and these waterways are accessible for longer periods of time each year. This possible increase in activity in the oceans around Canada could necessitate a larger defence presence and more search-and-rescue activity by both manned and unmanned ocean vehicles. This defence-oriented ocean activity by necessity must be covert: the communications must be undetectable by unintended listeners lest the position of the transmitters (for example, submarines) or the position or existence of receivers (for example, divers) be revealed. The necessity of covert communications between ships, submarines, divers, and unmanned surface and underwater vehicles requires highly resilient, relatively low power underwater communication techniques.

Covert underwater communication techniques are generally lower power, which also makes them more environmentally friendly. Low power means less energy consumption, helping organizations to meet green energy standard targets. The low-power signals could also be of benefit to the surrounding marine wildlife: the largest contributors to marine mammal deaths are collisions with ships, and stress due to ship noise [4]. Whales get stressed by the loud ship noise and flee to shallower waters where they wind up beached trying to escape the noise source. A low-power signal would be less intrusive to marine life and could reduce the risk of marine mammal injury.

The great challenge of covert communication is sending and receiving signals in such a way that only the intended target receives the signal.

1.1.1 Covert Underwater Communication

Covert communications fall into two different categories: low probability of detection (LPD), and low probability of interception (LPI). LPD typically involves transmitting the signal at low power so that it is below the noise floor (from the perspective of the receiver) to prevent detection by the instruments of any unintended listeners. This presents a unique challenge underwater because of the time-varying nature of the underwater channel: when channel conditions are poor, the user risks losing their own signal. Techniques to achieve LPD include spread-spectrum modulation, beamforming, and the use of waveforms resilient to time-variance. LPI involves designing signals which cannot be decoded even if they are discovered by a listener. Traditionally, this was done with complex coding schemes to make information difficult to decode once picked up by a listener. More recently, research has been done on transmitting code using biomimicry: hiding information in plain sight by attempting to mimic marine mammals. All of these approaches are valid, but the question remains: which approach is most valid for the operational environment?

In 2017, the JANUS protocol became the NATO standard for underwater acoustic communication [5]. JANUS is a robust protocol using Frequency Hopped Binary Frequency Shift Keying (FH-BFSK), but does not have very high bit rate. A comprehensive description of JANUS is detailed in Chapter 2.

In an attempt to improve bit rate, a technique with better spectral efficiency

like Orthogonal Frequency Division Multiplexing (OFDM) could be adapted to the JANUS protocol, but OFDM requires a comprehensive strategy for combating underwater channel impairments.

1.1.2 OFDM & Combating Channel Impairments

OFDM is a modulation technique where the total frequency band of the carrier signal is divided in to equally spaced sub-bands. The sub-carriers are spaced apart from each other such that one sub-carrier does not interfere with another sub-carrier. This is known as making the sub-carriers "orthogonal" to each other. Even though the sub-carriers have an overlap in frequency, the peak amplitude of one sub-carrier occurs when all other sub-carriers have an amplitude of 0. This allows you to maximize the spectral efficiency of your frequency band compared to FH-BFSK: frequency hopping requires using a much wider total band for each symbol because the symbols need to be able to hop frequency bands. At a given time T, FH uses a small portion of the available frequency band, whereas OFDM uses the whole frequency band. FH-BFSK means that you are only transmitting two symbols at a time: a 0 and a 1, using one of two carrier frequencies. One OFDM symbol can be broken down in to many multiple sub-carriers: in the new Wi-Fi 6 for example, OFDM can be used to modulate a 1024 QAM symbol. OFDM is also easy to equalize: it can be modulated and demodulated using the FFT, so when attempting to equalize a frequency-selective channel the operations boil down to direct matrix multiplication. This massive increase in throughput, on top of the ease of channel equalization, makes OFDM a desirable choice for air-to-air communication. However, there are a number of differences in the underwater channel that inhibit the efficient use of OFDM for underwater acoustic communication when compared to FH-BFSK. The major difference is that sound underwater travels at roughly 1500 m/s, which is much slower than radio waves in air travelling at roughly 3×10^8 m/s. This can result in insufficient channel coherence time, which causes unwanted Doppler effect.

Channel Coherence Time & Doppler Effect

The underwater acoustic channel is a time-varying channel for a large number of factors including changes in temperature, salinity, tides, turbidity, surface waves, and

rain, among other things. A major issue with the underwater acoustic channel is that motion of the receiver relative to the transmitter can be rapidly changing relative to the speed of the transmitted signal depending on the sea state, for example if the transmitter is fixed but the receiver is oscillating back and forth due to the motion of the ocean. Channel coherence time is the length of time which a channel remains invariant for all practical purposes. If a transmitted symbol has a transmission time that is longer than the coherence time of the channel, the transmission is subject to the Doppler effect, which causes the signal to spread in frequency. This frequency spreading can be very destructive for OFDM. In OFDM, the subcarriers are spread apart from each other at the minimum distance in frequency to allow for maximum spectral efficiency. If there are many subcarriers, the frequency difference between each subcarrier can be very small. If the frequency spreading of each subcarrier causes the subcarriers to overlap, the OFDM signal will experience inter-carrier interference (ICI). Combatting this ICI is key to improving multi-carrier modulation techniques for underwater communications. But how can we combat ICI? One interesting technique to look at is the chirp.

Chirps

A chirp is a signal which has a frequency that varies as a function of time. Linear frequency modulation (LFM) is when the chirp frequency varies linearly from high to low or low to high. LFM chirp signals have strong resilience to the Doppler effect because they occupy the entire frequency band and are recovered using a cross-correlation filter: even if the frequency of the transmitted signal spreads a little bit by the time it reaches the receiver, the frequency profile of the signal is similar enough to the reference that it can be easily recovered. Similar to OFDM, chirps can be spread apart from each other by altering their rate-of-change in frequency to make them orthogonal to each other when recovered using a cross-correlation filter. This technique is known as orthogonal chirp division multiplexing (OCDM), and is the main subject of this thesis. Chirps & OCDM are described in greater detail in Chapters 2 & 3.

1.2 Motivation

The motivation of this thesis is to enable a system that is flexible for both potential high throughput applications or potential covert applications.

Covert underwater communication techniques are typically highly reliable but very low throughput. With the improvement in sensor technology, specifically underwater imaging techniques, it is desirable to have a high throughput yet potentially still covert technique for transmitting larger amounts of data.

Techniques such as linear frequency modulation, or chirps, are highly resilient to the effects of the underwater channel, specifically the Doppler effect, but very low throughput. The multi-carrier modulation technique Orthogonal Frequency Division Multiplexing (OFDM) is very high throughput but very susceptible to the Doppler effect. Orthogonal Chirp Division Multiplexing is proposed as a technique to try and achieve the "best of both worlds". Proper implementation of this technique could result in a communication link that can be either high throughput or highly resilient to the underwater channel, making it a reliable way to transmit large amounts of data underwater with the flexibility to decrease throughput and increase covertness without simply increasing transmit power to overcome the effects of the underwater channel. Coding techniques could be applied to OCDM to increase covertness similar to how coding techniques are applied to chirps in [6],

1.3 Thesis Organization

The aim of this thesis is to investigate the viability of OCDM to implement a robust underwater communication technique to improve the throughput of standard practice covert techniques. For this purpose, the following objectives are defined.

1. Model the effect of channel and transmitter front-end impairments on multi-carrier modulation techniques;

2. Implement a pre-equalizer at the transmitter to increase throughput in a band-limited transmitter front-end;

3. Compare the performance of OCDM to standard OFDM; and

4. Evaluate the performance of both techniques in different measured conditions.

The rest of this thesis is organized as follows. Descriptions of other popular covert underwater communication techniques and impairments caused by the time-varying nature of the underwater channel are described in Chapter 2. Chapter 3 describes spread-spectrum techniques OFDM and OCDM, as well as work to compensate for the effects of a projector on the overall signal before transmission. The contributions of this thesis are discussed in Chapter 4: Chapter 4 compares the performance of OFDM and OCDM in both simulation in St. Margaret's Bay, and experiments run in the Dalhousie Aquatron in May 2021. Chapter 4 also proposes a pre-equalization technique done at the front-end of the transmitter which could allow for increased bandwidth, and decoupling of the equalization of the transmitter and receiver. Finally, chapter 5 draws conclusions from the results of the simulations and Aquatron experiment results and provides direction for future research.

Chapter 2

Description of Wireless Underwater Communication Techniques

Today, there is a demand for underwater wireless communication modulation techniques that are resilient to the effects inherent to the underwater acoustic channel, while also transmitting at low power to avoid disturbing marine life. Low Probability of Detection (LPD) is an extremely important characteristic for military underwater communication systems. In [7], a variety of LPD communication techniques are described: spread-spectrum techniques like direct-sequence spread-spectrum [8] and frequency hopping [9] are susceptible to the Doppler shift, but Doppler shift compensation techniques are well documented for Linear Frequency Modulation (LFM) [10]. Note that standard LFM can also be intercepted at high SNR. One method of hiding high-power LFM is by mimicking marine mammal acoustic signatures in a process known as biomimicry.

In Section 2.1, the definition of LPD and LPI communications is provided. Then, different potential techniques to enable LPD and LPI are reviewed. Specifically, in Section 2.2, artificial waveforms that can resemble those of marine mammals are described. Then, in Section 2.3, the use of chirps for LPI are described; Section 2.4 describes spread spectrum techniques. In Section 2.5, the JANUS protocol is described because it is intended to be a standard adopted by underwater manufacturers. Finally, in Section 2.6, the possibility and challenges for providing directivity using beamformers at the transmitter is reviewed.

2.1 Low Probability of Detection and Interception

Covert communications fall into two different categories: low probability of detection (LPD), and low probability of interception (LPI). Figure 2.1 provides a visual aid for when it is appropriate to use LPI or LPD. LPI communication is necessary when the eavesdropper is inside the white circle closer to the transmitter. LPD communication

is more suitable inside the grey region, when the eavesdropper is nearer to the intended receiver. Within a specific range of the transmitter, it is too difficult to make a signal undetectable by an eavesdropper. The signal will almost certainly be detected, and LPI systems are required to prevent an intruder from decoding the message, even when the signal can be detected by the instrumentation of an eavesdropper. At a greater distance away from the transmitter, it is much easier to hide the presence of the transmit signal from eavesdroppers and marine mammals. As such, LPD systems increase the range at which the instrumentation of an intended receiver can detect a transmit signal.

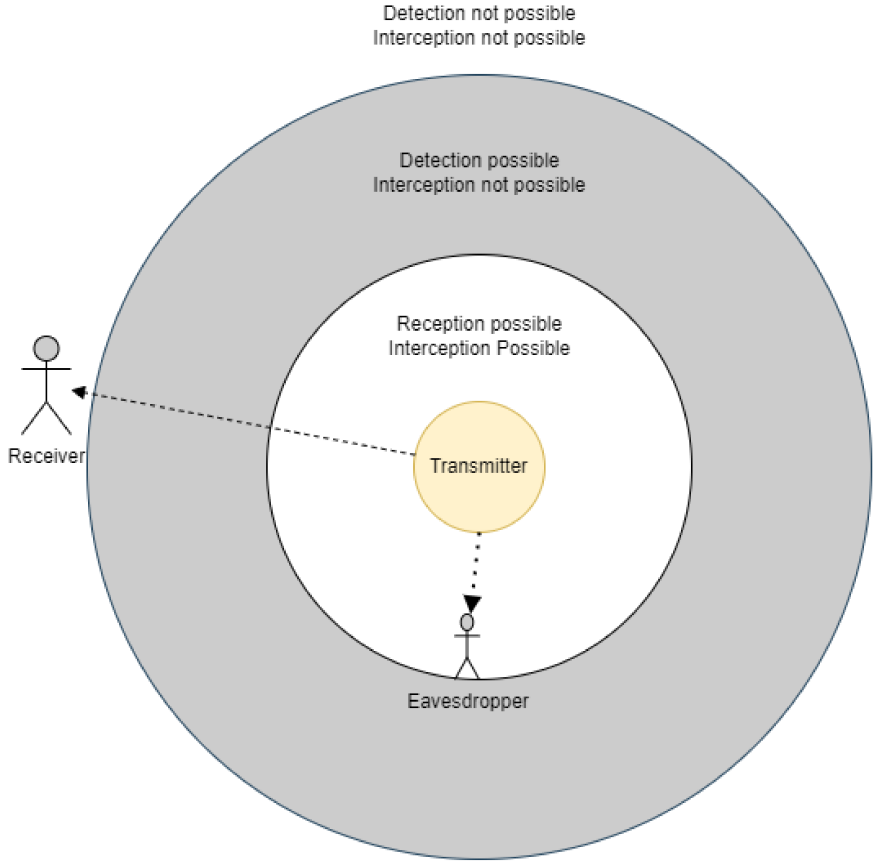

Figure 2.1: Illustration of the differences between LPD and LPI.

LPD systems present a unique challenge underwater because of the time-varying nature of the underwater channel: when channel conditions are poor, there is a risk that the intended receiver will not receive the transmit signal. Techniques to achieve LPD include spread-spectrum modulation, which will be described in Section 2.4,

beamforming described in Section 2.6, and the use of waveforms resilient to time-variance, such as the chirp described in Section 2.3.

LPI involves designing signals which cannot be decoded even if they are detected by an eavesdropper. Traditionally, this is done with complex coding schemes to make information difficult to decode once it is detected by an eavesdropper. More recently, research has been done on transmitting code using biomimicry: hiding information in plain sight by attempting to mimic marine mammals. Biomimicry will be described next.

2.2 Biomimicry

Biomimicry [11] is the use of mathematical models and technological innovation to imitate processes found in nature for the purposes of solving human problems. In the context of covert underwater communication, biomimicry involves imitating marine mammal vocalizations to fool eavesdroppers into thinking that the signal they are listening to is a part of the natural environment. For example, in [12], a modulation technique is described using a continuously varying carrier frequency to imitate dolphin whistles. To mimic marine mammal signatures, the characteristics must first be understood.

In August 2019, a sea trial experiment was undertaken in Grand Passage, Nova Scotia, in the Bay of Fundy to understand local marine mammal vocalizations. A passive horizontal array of acoustic sensors was deployed for one week and marine mammal vocalizations were recorded for 12-hour periods each day.

The recorded signatures include whale and dolphin vocalizations, and whale, dolphin and harbour porpoise clicks. Table 2.1 summarizes the frequency range for which three different marine mammals were recorded. Figure 2.2a shows the spectrogram of a dolphin whistle. Figure 2.2b shows a similar spectrogram for a humpback whale song. These vocalizations show up as vertical sweeps on a spectrogram: they change in frequency over time. Figure 2.2c shows a time series of harbour porpoise clicks at ultrasonic frequencies.

One way to use these signatures in covert communication would be to record them, and then transmit them at very high power while also transmitting another signature, such as FSK, at much lower power in the same frequency band, so that only

Table 2.1: Marine Mammal Acoustic Signatures Characteristics

	Signature	Frequency Range (kHz)
Humpback Whale	Whistle	2-10
Dolphin	Whistle	8-15
Harbour Porpoise	Clicks	120-140

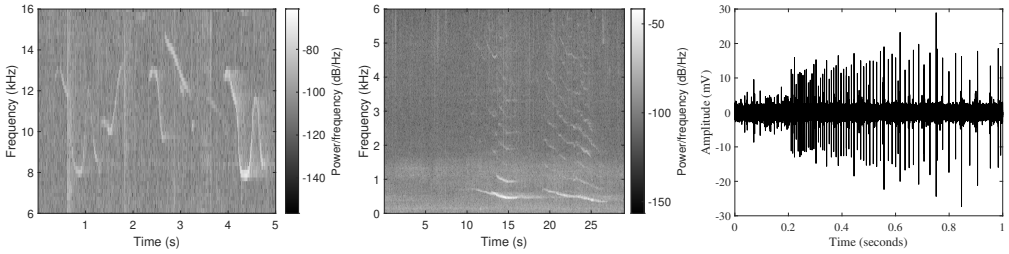

(a) Dolphin whistle. (b) Humpback whale call. (c) Harbour porpoise clicks.

Figure 2.2: Marine mammal vocalizations and echolocations in the Bay of Fundy.

the mammal signatures show up on listening instruments and the actual information signal just looks like noise. A receiver in such a communication system would need to have a very powerful matched filter in order to make sure that it decodes the intended information signal while ignoring the marine mammal recording. Another method would be to use the different marine mammal signatures themselves to carry the information. In [13], a dolphin whistle is used for synchronization, and dolphin clicks are used to carry information: the time between clicks determines the information bit. In [12], a dolphin whistle is mimicked by continuously varying the carrier frequency of the transmit signal, using differential binary phase-shift keying (DBPSK) for the transmit data, resulting in a recoverable signal that looks almost exactly like a dolphin whistle. In order to mimic the animals in this way, a large number of different signatures would need to be recorded and used intermittently to prevent the full transmit signature from looking unnatural, therefore hinting to an unintended listener that what they are detecting is not actually a mammal. The high-power nature of these transmissions is now a double-edged sword: if the transmitter is sufficiently far away from an eavesdropper, they may intentionally avoid it thinking that it is a marine mammal. However, if the eavesdropper is skeptical, it now becomes much

easier for them to pinpoint the exact location of the transmitter. Thus it can be said that many biomimicry approaches focus more on LPI than LPD. If a low power signal to maintain LPD is desirable, it may be more prudent to focus on chirps, or chirp spread-spectrum (CSS).

2.3 Chirps

A chirp is a signal which has a frequency that varies as a function of time. For example, a linear chirp, also known as linear frequency modulation, is generated by

$$\psi(t) = e^{j(\pi a t^2 + 2\pi\beta t + \varphi_0)} \tag{2.1}$$

where a is the chirp rate of the frequency function, or how much the frequency changes with respect to time, β is the carrier frequency, and φ_0 is initial phase. Figure 2.3 shows a visual representation of a chirp.

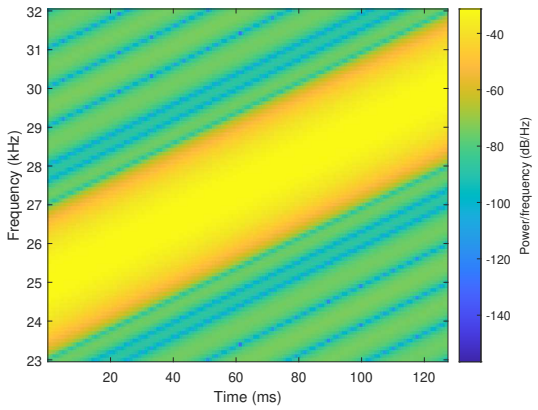

Figure 2.3: Spectrogram of a chirp that increases linearly in frequency over time.

According to [6], chirp transmissions have characteristics that appear to ideally address the requirements of an LPI/LPD scheme. First, their possible high processing gain (time-bandwidth product) and resilience against severe channel effects like multipath, scattering, and Doppler effect, enables high LPD/LPI performance since robust reception performance under low signal-to-noise (SNR) conditions reduces the need for high transmission power. Second, the wideband nature of chirp signals results in high LPD/LPI performance since the low power spectral density reduces the probability of detection and intercepts. Third, chirp signals are ubiquitous in the

underwater environment. Therefore, they cannot be easily associated with a specific communication system. This third trait allows for innovative solutions to LPI communication like shaping chirps to imitate dolphin clicks, or transmitting chirps at the same time as pre-recorded dolphin clicks, to hide the signal in "plain sight" as mentioned in the previous section.

One disadvantage of chirps is that because they are wideband and are a single-carrier modulation technique, they have low bit rate per symbol. Linear chirps, for example, only have a bit rate of 1 bit per symbol (either up or down i.e. one or zero).

Chirps are chosen over traditional spread spectrum methodologies due to their relative simplicity and high resilience to the effects of Doppler shift in the underwater channel. To test the properties of chirps, a sea trial was conducted in July 2019 in a very shallow (5 m depth, near-field effects not considered during the initial experiment) channel in a strait near Halifax, Nova Scotia, as well as in the Bay of Fundy near Grand Passage, Nova Scotia. Binary LFM chirps were transmitted on a 27 kHz sine wave carrier, encoded with a pseudo-random noise (PRN) sequence. Five PRN sequences were transmitted over a period of 5 minutes for a total of 20475 transmitted bits at a bit rate of 78 bits/s.

Table 2.2: Summary of Sea Trial Transmission Loss and BER

Deployment Scenario		Halifax Arm (200 meters)	Halifax Arm (500 meters)	Grand Passage (200 meters)
Transmission Loss (dB)		94.9	113.3	55.1
		Bit Error Rate		
Number of Sensors	1	0.0138	0.0142	0.0012
	2	0.0020	0.0059	4.8840e-05
	3	2.8840e-5	0.0023	0
	4	0	0.0013	0
	5	0	0.0011	0

The reliability of the communication link was evaluated over a distance of 200 m, and 500 m. The receiver consisted of 5 hydrophones in a vertical array. From Table 2.2, it can be seen that the transmission loss in the channel is extremely high for such short distances. This is much lower than predicted by simulation, and is attributed to the very shallow conditions, on the order of 5 metres. The channel was also subject

to frequent noise from power speed boats throughout the experiment, which explain the change of in-band energy as shown in Figure 2.4a at around 250 seconds.

Despite the poor channel conditions, data was able to be successfully recovered. After filtering out-of-band noise, the presence of in-band noise can still be seen for the 500 m trial in Figure 2.4a. A single hydrophone is shown as a representation of the signal on a given receiver. During measurements, 5 elements were recording data. The filtered signal was cross-correlated with a binary LFM chirp reference. Figure 2.4b shows an example of the cross-correlation after performing equal gain combining on the 5 received channels. The blue peaks represent a 1, and the orange peaks represent a -1. This experiment was then repeated in Grand Passage, Nova Scotia, at a distance of 200 m in a channel with a more reasonable transmission loss, and the BER improved dramatically. Table 2.2 shows the bit error rate (BER) for each trial after equal gain combining. The recovered signals had minimum BERs of 0 at 200 m with 4 receivers, and 1e-3 at 500 m with 5 receivers in the presence of pleasure craft noise and a channel transmission loss of over 113 dB. In Grand Passage, the BER was 0 with just two receivers.

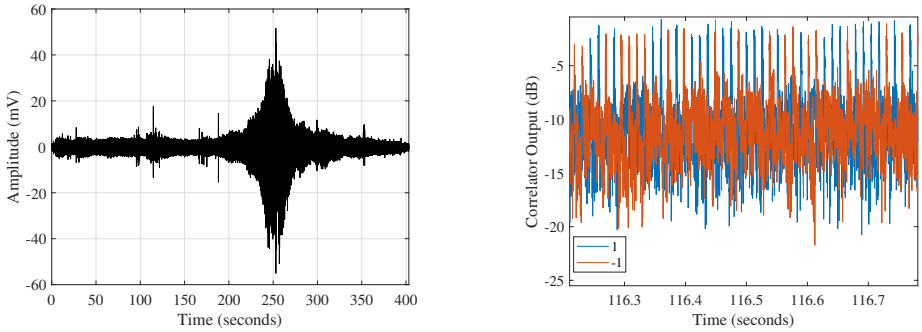

(a) LFM Signal after filtering noise (b) Decoded signal

Figure 2.4: Received data in Halifax Arm at 200m.

The reliability of the chirp signal in the presence of such huge transmission losses indicates that the LFM chirp may be an ideal technique for LPD communication. However, the data rate of such a signal is very low, so it may be desirable to investigate other methods.

2.4 Spread Spectrum Techniques

Spread spectrum techniques can be used to provide LPI communication links underwater. [14] gives a good overview of two major spread spectrum techniques: direct-sequence spread spectrum (DSSS) and frequency-hopping spread spectrum (FHSS).

Direct-Sequence Spread Spectrum

In direct-sequence spread spectrum, the transmitted information bits are spread out in frequency by multiplying each information bit by a pseudo-noise (PN) sequence. Each element of the PN sequence is called a chip. The chips are much shorter in duration than an information bit, so the chip rate of the PN sequence is much higher than the bit rate of the information signal. Since the chips occupy the same bandwidth as the information bit, this spreads the energy of the signal out over the whole bandwidth, resulting in a much lower power signal: the DSSS signal looks similar to white noise. The receiver has a reference of the PN-sequence, and "despreads" the signal using a cross-correlation operation. The result is a signal that can potentially be transmitted below the noise floor (even while the transmission itself contributes to noise from the perspective of any unintended receivers) and recovered successfully at the receiver while not being an obviously detected signal when observed by an eavesdropper. Even if the signal is intercepted, the signal cannot be recovered without the PN-sequence as a reference. One problem with DSSS is that it is very susceptible to Doppler shift and therefore requires very accurate time-synchronization [7]. DSSS also happens to be very slow underwater because the frequencies at which it works best for LPD communication are very low (on the order of 100 Hz) [14].

Frequency-Hopping Spread Spectrum

Another spread spectrum method is to spread the signal in frequency using frequency hopping. In frequency hopping, the transmit signal carrier frequencies change according to a PN-sequence: each set of carrier frequencies is narrowband compared to the overall bandwidth of the channel: each chip is transmitted on a different carrier. The frequency hopping is typically applied to FSK or PSK modulation. In this way, an interceptor might only see one chip, not the entire signal: without knowing the

hopping pattern, it is difficult for an interceptor to recover. This also makes the signal difficult to jam, since the jammer doesn't know exactly which frequency bands to interfere with and would need a very powerful wideband jammer. So long as the chip duration is longer than the multipath channel arrival time, and the bandwidth of a chip is much smaller than the bandwidth of the channel, the channel can be said to be frequency flat (non-fading) within the bandwith of a single chip. This makes FHSS resilient to multipath fading. However, much like DSSS, FHSS is also susceptible to Doppler shift [7] and works best at very low frequencies and data rates [14].

The same things that make FHSS good at LPI communication also make it good for multiple access: since chip durations are very short and narrowband, intersymbol interference is minimized. FH-BFSK is the technique used in JANUS, the NATO standard for underwater acoustic communications.

2.5 JANUS

The JANUS standard for underwater acoustic communication [15] was developed by NATO in 2017 [5]. The purpose of JANUS is to solve the problem of interoperability between modems and assets from different manufacturers. Prior to JANUS, underwater modems typically used communication protocols that were proprietary to their manufacturers: there was little ability for devices from different manufacturers to talk to each other, preventing the creation of ad-hoc networks. Designed to be robust and simple to implement, JANUS employs FH-BFSK with 13 evenly-spaced subcarrier pairs. Robustness to time and frequency fading is provided by a 1/2 convolutional encoder and interleaving. Data integrity is maintained by an 8-bit cyclic redundance check (CRC). The tradeoff for this reliability is speed and bandwidth: JANUS has a centre frequency of 11520 Hz, and a total bandwidth of 4160 Hz. Its chip duration is 6.25 ms and it has a bit rate of 80 bps. Increasing the centre frequency and bit rate has been attempted [16], but this drastically reduces the reliability of the communication link over longer distances. JANUS also suffers from the previously identified FHSS problem of being susceptible to Doppler shift. As a technique for LPD/LPI communication, while JANUS has the advantages of FHSS, it also has the disadvantage of being open-source: JANUS is intended to be widely adopted by both

military and civilian operations. This open-source nature makes it difficult to justify as a covert technique because it is known by everyone and intended to be easily recognizable.

The two major problems of JANUS and other previously mentioned spread-spectrum techniques, is that they are low bit-rate and susceptible to Doppler shift. The previously mentioned LFM chirp is highly resilient to the Doppler effect, but is still low bit-rate. Chapter 3 investigates the multicarrier OFDM as a method for improving bit rate, but OFDM is still susceptible to the Doppler effect. OCDM is investigated as an alternative to OFDM, combining the principle of OFDM with chirps to provide a multicarrier modulation technique that is more resilient to Doppler while maintaining high bit-rates.

2.6 Providing Directivity

Before we move on to multi-carrier modulation techniques, it is worth mentioning the impact that providing directivity can have on the covertness of a signal. Beamforming is a spatial diversity technique that can be used to direct acoustic energy towards a point of interest. Instead of all acoustic energy radiating outwards in all directions equally, the acoustic energy has high intensity only along the line of sight between transmitter and receiver. When appropriately beamformed, the intensity of the acoustic energy is greatly reduced in all directions other than the line of sight. This directivity assists with the covertness of the signal: the less energy there is outside of the communication line of sight, the less likely an eavesdropper will be to detect the signal unless they are directly in the path of the signal.

Though not the focus of this research, beamforming is an important part of underwater communication and its application to covert underwater communication should be studied in greater detail in future research.

Chapter 3

Multi-carrier Modulation Techniques

3.1 Transmitting OFDM Underwater

Orthogonal Frequency-Division Multiplexing (OFDM) takes advantage of the Fourier transform and the mathematical concept of orthogonality to transmit multiple subcarriers on one frequency band. It is popular in telecommunications standards such as Wifi and 5G. OFDM can be thought of as an implementation of frequency-division multiplexing that maximizes the spectral efficiency of the transmitted signal. The simplest OFDM modulation scheme can be seen in Figure 3.1.

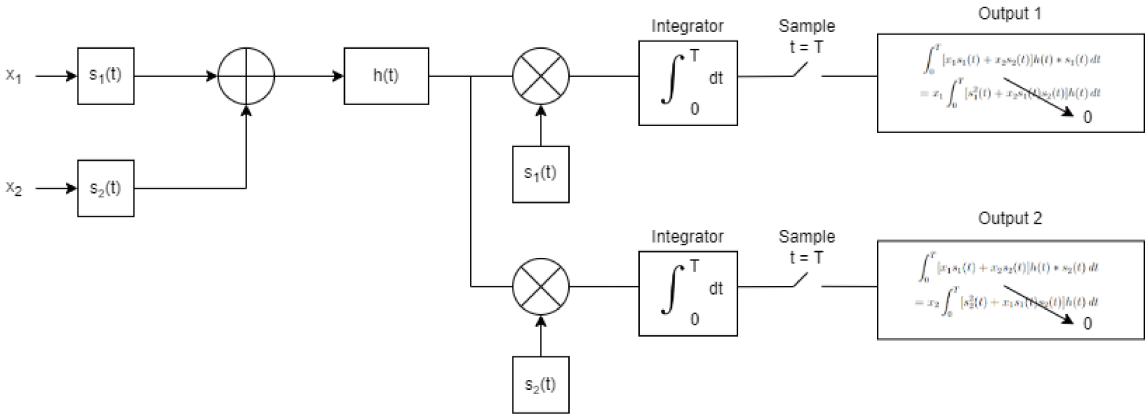

Figure 3.1: A visual representation of OFDM.

The signals s_1 and s_2 are sine waves at distinct carrier frequencies. Each subcarrier is modulated by a unique message, represented in Figure 3.1 by x_1 and x_2. The subcarriers are added together, transmitted across the channel $h(t)$, and then demodulated using a multiplier and integrator. When the received signal is multiplied by a subcarrier at the receiver, the other subcarriers are cancelled out. This is the concept of "orthogonality" in OFDM: all of the subcarriers can be transmitted within the same band without interfering with each other, because multiplying two subcarriers together cancels them out. In practice, the sub-carrier spacing is fixed,

and mathematically the transmit signal $x(t)$ with N subcarriers can be expressed as

$$x(t) = \sum_{k=0}^{N-1} X_k e^{j(2\pi k/T)t}, \tag{3.1}$$

which is the equation for the discrete Fourier transform. This is very helpful in the implementation of the modulator, the demodulator, and equalizer in discrete-time, as will be demonstrated.

From [17], consider a single-input single-output system with a bandwidth B, and a frequency selective channel-impulse response $h[l](l = 0, 1, \ldots, L-1)$ where L is the length of the channel. Let $x[k](k = 0, 1, 2, \ldots, N-1)$ be a sequence of N data symbols to be transmitted, typically represented with Quadrature Amplitude Modulation (QAM) at the input of the OFDM transmitter. The data sequence is represented as an $N \times 1$ vector $\boldsymbol{s} = [s[0], s[1], \ldots, s[N-1]]^T$. An Inverse Fast Fourier Transform (IFFT) is applied on the transmit sequence, generating the vector $\tilde{\boldsymbol{s}} = [\tilde{s}[0], \tilde{s}[1], \ldots, \tilde{s}[N-1]]^T$. Linear algebra can be used to represent $\tilde{\boldsymbol{s}}$ by

$$\tilde{\boldsymbol{s}} = \boldsymbol{D}^H \boldsymbol{s} \tag{3.2}$$

where $\boldsymbol{D}^H$ is the Hermitian of matrix $\boldsymbol{D}$, which is an $N \times N$ matrix whose (m, n)-th $(m, n = 1, 2, \ldots, N)$ element is given by

$$[\boldsymbol{D}]_{m.n} = \frac{1}{\sqrt{N}} e^{-\frac{j2\pi(m-1)(n-1)}{N}}. \tag{3.3}$$

In practice, N is chosen to be a power of 2 (64-1024 are commonly used). A cyclic prefix, CP, is pre-pended to $\tilde{\boldsymbol{s}}$, to obtain the transmit sequence, $\boldsymbol{s'}$. The CP is made of the last $L-1$ symbols of $\tilde{\boldsymbol{s}}$. So the full transmit sequence is $\boldsymbol{s'} = [\tilde{s}[N-L+1], \ldots, \tilde{s}[N-1], \tilde{s}[0] \ldots, \tilde{s}[N-1]]^T$. The vector $\boldsymbol{s'}$ is known as the OFDM symbol and has a duration of $T_s^{OFDM} = (N + L - 1)/B$.

The receiver, at baseband, acquires the sequence $\boldsymbol{y'}$ which is a vector with length $(N+2L-2)$, and is a convolution of the transmit OFDM symbol $\boldsymbol{s'}$ with the channel of length L. The CP is removed, leaving us with N samples of the received signal, $\tilde{\boldsymbol{y}} = [y'[0], y'[1], \ldots, y'[N-1]]^T$ that satisfy

$$\tilde{\boldsymbol{y}} = \sqrt{E_s}\tilde{\boldsymbol{H}}\boldsymbol{s'} + \tilde{\boldsymbol{\psi}}, \tag{3.4}$$

where E_s is the average energy available at the transmitter over time T_s, $\tilde{\boldsymbol{\psi}}$ is the additive noise from the channel, and $\tilde{\boldsymbol{H}}$ is an $N \times (N+L-1)$ Toeplitz matrix derived from the channel impulse response and is given by

$$\tilde{\boldsymbol{H}} = \begin{bmatrix} h[L-1] & \cdots & h[1] & h[0] & 0 & 0 & \cdots & 0 \\ 0 & h[L-1] & \cdots & h[1] & h[0] & 0 & \cdots & 0 \\ \vdots & 0 & \ddots & \ddots & \ddots & \ddots & \ddots & \vdots \\ 0 & \vdots & 0 & h[L-1] & \cdots & h[1] & h[0] & 0 \\ 0 & 0 & 0 & 0 & h[L-1] & \cdots & h[1] & h[0] \end{bmatrix}. \tag{3.5}$$

Taking advantage of the fact that the first $L-1$ samples of $\boldsymbol{s}'$ are identical to the last $L-1$ samples of $\boldsymbol{s}'$ due to the CP, (3.4) can be simplified to

$$\tilde{\boldsymbol{y}} = \sqrt{E_s}\boldsymbol{H}_c\tilde{\boldsymbol{s}} + \tilde{\boldsymbol{\psi}}, \tag{3.6}$$

where

$$\boldsymbol{H}_c = \begin{bmatrix} h[0] & 0 & \cdots & 0 & 0 & h[L-1] & \cdots & h[1] \\ h[1] & h[0] & 0 & \cdots & 0 & 0 & \ddots & \vdots \\ \vdots & h[1] & h[0] & 0 & 0 & \ddots & 0 & h[L-1] \\ h[L-1] & \vdots & h[1] & \ddots & 0 & \ddots & 0 & 0 \\ 0 & h[L-1] & \vdots & \ddots & h[0] & \ddots & \ddots & 0 \\ \vdots & 0 & h[L-1] & \ddots & h[1] & h[0] & 0 & 0 \\ \vdots & \vdots & 0 & \ddots & \vdots & \ddots & \ddots & 0 \\ 0 & 0 & \cdots & 0 & h[L-1] & \vdots & h[1] & h[0] \end{bmatrix}. \tag{3.7}$$

The CP makes the $N \times N$ matrix $\boldsymbol{H}_c$ circular. This allows $\boldsymbol{H}_c$ to be simplified as

$$\boldsymbol{H}_c = \boldsymbol{D}^H\boldsymbol{\Omega}, \tag{3.8}$$

where $\boldsymbol{\Omega} = \text{diag}[\omega[0], \omega[1], \ldots, \omega[N-1]]$, with

$$\omega[k] = \sum_{l=0}^{L-1} h[l]e^{-\frac{j2\pi kl}{N}}, k = 0, 1, 2, \ldots, N-1. \tag{3.9}$$

Eq. (3.9) is the channel frequency response of the channel, where k represents the subcarrier index. Upon receiving the signal, the receiver performs an FFT on $\tilde{\boldsymbol{y}}$ to obtain

$$\boldsymbol{y} = \boldsymbol{D}\tilde{\boldsymbol{y}}, \tag{3.10}$$

where $\boldsymbol{y} = [y[0], y[1], \ldots, y[N-1]]^T$. Combining (3.2), (3.6), (3.8), and (3.10) produces the frequency domain input-output relationship of the channel which can be expressed as

$$\boldsymbol{y} = \sqrt{E_s}\boldsymbol{D}\boldsymbol{D}^H\boldsymbol{\Omega}\boldsymbol{D}\boldsymbol{D}^H\boldsymbol{s} + \boldsymbol{D}\tilde{\boldsymbol{n}} = \sqrt{E_s}\boldsymbol{\Omega}\boldsymbol{s} + \boldsymbol{n}, \tag{3.11}$$

where $\boldsymbol{n} = \boldsymbol{D}\tilde{\boldsymbol{n}}$. $\boldsymbol{D}$ is a unitary matrix ($\boldsymbol{D}\boldsymbol{D}^H = \boldsymbol{I}_N$). Eq. (3.11) shows that using a CP, with an IFFT at the transmitter and an FFT at the receiver, the frequency selective channel can be split in to N parallel flat fading channels each with a bandwidth of B/N. The data symbol on the kth subcarrier, using (3.11) is

$$y[k] = \sqrt{E_s}\omega[k]s[k] + n[k], k = 0, 1, 2, \ldots, N-1. \tag{3.12}$$

In practice, OFDM is implemented to maintain a low-complexity equalization in wideband systems, while maintaining reliability. Comparing OFDM to, for example, the LFM chirp technique in Chapter 2, if a chirp occupies a given bandwidth B, only one bit of information is transmitted with each symbol. With OFDM, that same bandwidth B can be subdivided into N sub-carriers, multiplying the number of transmitted data symbols by N over that same time period. Compared to a spread spectrum technique such as FHSS, which also divides the total bandwidth of the channel in to multiple sub-bands, at any given time OFDM occupies all sub-bands at once as opposed to just a single sub-band. In other words, OFDM is much more spectrally efficient than the techniques mentioned in Chapter 2. It can be noted that spread spectrum can be applied with OFDM (this is sometimes referred to as multi-carrier modulation), to create redundancy in the frequency domain [18].

The orthogonality of OFDM can be deteriorated by the Doppler effect. Doppler shift occurs when the received frequency increases or decreases slightly over time relative to the transmitter. This is typically caused by relative movement between

transmitter and receiver. Doppler spreading occurs when multiple paths of the signal arrive each with different Doppler shifts. With OFDM, Doppler spreading in the subcarriers can cause inter-carrier interference (ICI). ICI is caused by a change in frequency which causes subcarriers to overlap each other, losing their orthogonality with one another. This is investigated in more detail in Section 3.2.

3.2 OFDM & Doppler Spread

As stated in Section 3.1, OFDM underwater is very susceptible to Doppler spread. In [19], a model is presented that includes the effect of Doppler shift and Doppler spread on OFDM. Doppler shift is a change in frequency when there is relative motion between a sound source and a listener. This change in frequency can be described as

$$\Delta f = f_0(\Delta v_p/c), \tag{3.13}$$

where Δf is the Doppler shift, f_0 is the nominal frequency of the sound source, Δv_p is the relative velocity between the sound source and the listener along path p, and c is the speed of propagation of sound waves in the medium along path p In this case, c is the speed of sound in water [20].

To assess the Doppler effect on OFDM, we first reexamine (3.7). The matrix $\boldsymbol{H_c}$ implements the circular convolution between the channel and a signal with a cyclic prefix. Converting $\boldsymbol{H_c}$ into the frequency domain via Fourier transform diagonalizes the circulant matrix, producing

$$\begin{aligned} \boldsymbol{Y} &= \boldsymbol{F}^H \tilde{\boldsymbol{y}} \\ &= \boldsymbol{F}^H \boldsymbol{H_c} \boldsymbol{F} \boldsymbol{s} + \tilde{\boldsymbol{\psi}}) \\ &= \boldsymbol{\Gamma} \boldsymbol{s} + \boldsymbol{\Psi}, \end{aligned} \tag{3.14}$$

where $\boldsymbol{s}$ is the transmit data symbol in the frequency domain and $\boldsymbol{\Psi}$ represents noise. $\boldsymbol{\Gamma}$ is analogous to (3.8), but using the discrete Fourier transform matrix $\boldsymbol{F}$ instead of the FFT matrix $\boldsymbol{D}$. Let's define $\boldsymbol{\Gamma}$

$$\boldsymbol{\Gamma} = \boldsymbol{F^H H_c F} = \begin{bmatrix} \boldsymbol{H_c}[0] & & \\ & \ddots & \\ & & \boldsymbol{H_c}[N-1] \end{bmatrix}. \tag{3.15}$$

Note that $\mathbf{\Gamma}$ is a diagonal frequency gain matrix, and the received signal vector $\tilde{\boldsymbol{y}} = [y[0] \cdots y[N-1]]^T$ at index n is

$$\tilde{y}[n] = \frac{1}{\sqrt{N}} \sum_{k=0}^{N-1} H_c[k] s[k] e^{j2\pi kn/N} + \tilde{\psi}[n]. \tag{3.16}$$

Demodulating using the DFT produces a vector $\boldsymbol{Y}[k]$. Its value at index k is equal to

$$Y[k] = \frac{1}{\sqrt{N}} \sum_{n=0}^{N-1} y[n] e^{-j2\pi kn/N} = H[k] s[k] + \psi[k]. \tag{3.17}$$

It is important to note that when the Doppler effect is present, (3.15) is no longer diagonal: the non-diagonal elements represent the Doppler shift.

To examine this in greater detail, we first look at the impulse response of a multipath channel

$$h(t, \tau) = \sum_{p=1}^{P} A_p(t) \delta(\tau - \tau_p(t)), \tag{3.18}$$

where p is the path, t is time, τ_p is delay along path p, and A_p is the amplitude of the path arrival. For this scenario, let's make the following three assumptions for a given OFDM symbol i:

1. The amplitude of path p is constant during the transmission of symbol i ($A_{p,i}(t) = A_{p,i}$), since the variation in distance is relatively small compared to the original distance.

2. The delay variation for each path can be approximated as $\tau_{p,i}(t) = \tau_{p,i} - a_{p,i}t$ where $a_{p,i}$ is the relative change in frequency $\Delta v_{p,i}/c$ of path p. This is a reasonable assumption, since the duration of each symbol is relatively small, in comparison to the direction and the acceleration of a platform.

3. The symbol duration T is less than coherence time of the channel T_{coh}. Typically, the coherence time is on the order of 100 msec, and this assumption is valid for short OFDM symbols.

The impulse response for symbol i then becomes

$$h_i(t) = \sum_{p=1}^{P} A_{p,i} \delta((1 + a_{p,i})t - \tau_{p,i}). \tag{3.19}$$

Assumption number 3 can be confirmed by channel sounding and then adjusting the transmission symbol duration accordingly. Because $T > T_{coh}$, the channel gains are assumed to be time-invariant within a single OFDM block, so time t has been replaced by the block index i. Channel gains $A_{p,i}$ are approximately constant per block.

Converting to the frequency domain shows that the channel phases are not time-invariant like the path amplitudes. Performing an FFT on (3.19), the channel frequency response for OFDM symbol i is

$$H_i(f) = \sum_{p=1}^{P} |A_{p,i}| e^{-j2\pi f \tau_{p,i}/(1+a_i)}, \tag{3.20}$$

which shows that each path p has a different phase shift at different frequencies. The received signal $y_i(t)$ consists of the sum of the delayed and compressed copies of the transmit signal $s_i(t)$

$$\begin{aligned} y_i(t) &= \tilde{s}_i(t) * h_i(t) + \tilde{\psi}_i(t) \\ &= \sum_{p=1}^{P} A_{p,i} s_i((1+a_{p,i})t - \tau_{p,i}) + \tilde{\psi}_i(t). \end{aligned} \tag{3.21}$$

Examining a single path p, the transmit signal $s(t)$ is

$$s(t) = Re\left\{ \sum_{n=0}^{N-1} x[n] g(t - nT/N) e^{j2\pi k f_c t} \right\}. \tag{3.22}$$

The received signal on path p after matched filtering with a pulse filter $g(-t)$ is

$$r_{p,i}(t) = Re\left\{ A_{p,i} \sum_{n=0}^{N-1} x[n] q((1+a_i)t - nT/N - \tau_{p,i}) e^{j2\pi f_c (1+a_i) t} \right\} \tag{3.23}$$

Eq. (3.22) is down-converted to baseband with a local copy of the carrier signal $e^{-j2\pi k f_c t}$, producing a received signal

$$y_{p,i} = r_{p,i} e^{-j2\pi k f_c t} = A_{p,i} \sum_{n=0}^{N-1} x[n] q((1+a_i)t - nT/N - \tau_{p,i}) e^{j2\pi f_c (1+a_i) t} e^{-j2\pi k f_c t} \tag{3.24}$$

In order to properly synchronize the received signal, $y_{p,i}$ is sampled at a sample time $t = n'T_c/(1+a_i)$, and the discrete sampled received signal is

$$y_i[n'] = y_{p,i}\left(\frac{n' T_c}{1+a_i} \right) = A_{p,i} \sum_{n=0}^{N-1} x[n] q\left(\frac{(n'-n)T}{N} - \tau_{p,i} \right) e^{j2\pi f_c n' \frac{a_i}{1+a_i} \frac{T}{N}}. \tag{3.25}$$

Let $q_{p,n'-n} = q\left(\frac{(n'-n)T}{N} - \tau_{p,i}\right)$ and $V = e^{j2\pi f_c \frac{a_i}{1+a_i}\frac{T}{N}}$. Then, (3.25) becomes

$$y_i[n'] = A_{p,i} V^{n'} \sum_{n=0}^{N-1} x[n] q_{i,n'-n}. \tag{3.26}$$

In OFDM, discrete samples $x[n]$ are generated by performing an IFFT on discrete data symbols $X[k]$. Defining $W = e^{j2\pi/N}$, (3.25) can be written as

$$y_i[n'] = A_{p,i} V^{n'} \sum_{n=0}^{N-1} q_{i,n'-n} \sum_{n=0}^{N-1} X[k] W^{nk}. \tag{3.27}$$

Written in vector form, the output of the IFFT for symbol i becomes

$$\tilde{\boldsymbol{y}}_{\boldsymbol{i}} = A_{p,i} \boldsymbol{V} \boldsymbol{H} \boldsymbol{F} \boldsymbol{x}, \tag{3.28}$$

where $\boldsymbol{V} = \text{diag}\{1, V, V^2, \cdots, V^N - 1\}$ is the chirp transform, $\boldsymbol{F} = W^{nk}$ is the discrete Fourier transform, and $\boldsymbol{H} = \boldsymbol{H_c}$ from (3.8) with entries $q_{i,j} = g_j$. Applying an FFT to $\boldsymbol{y_i}$, we obtain

$$\boldsymbol{y}_i = \boldsymbol{F}^H \tilde{\boldsymbol{y}}_{\boldsymbol{i}} = A_{p,i} \boldsymbol{F}^H \boldsymbol{V} \boldsymbol{F} \boldsymbol{F}^H \boldsymbol{H} \boldsymbol{F} \boldsymbol{x}. \tag{3.29}$$

In (3.29), there is a time selective term which characterizes the Doppler shift and can demonstrate intercarrier interference

$$\boldsymbol{V}^{(f)} = \boldsymbol{F}^H \boldsymbol{V} \boldsymbol{F}, \tag{3.30}$$

and there is a frequency selective term

$$\boldsymbol{H}^{(f)} = \boldsymbol{F}^H \boldsymbol{H} \boldsymbol{F}. \tag{3.31}$$

The ICI manifests as a circulant interference pattern among the frequency domain symbols of $\boldsymbol{X}$.

Adding all the paths together produces the fully received OFDM symbol block

$$\boldsymbol{y}_i = \sum_{p=1}^{P} A_{p,i} \boldsymbol{F}^H \boldsymbol{V}_{p,i} \boldsymbol{F} \boldsymbol{H}_p^{(f)} \boldsymbol{x}. \tag{3.32}$$

The effect of Doppler shift on the signal can then be isolated and investigated by changing the value of $a_{p,i}$. For example, consider a single OFDM block with 5

paths and all path amplitudes equal to 1 ($i = 1$ and $A_{p,1} = 1$). Assume also that the frequency-selective portion of the channel, $\boldsymbol{H}_p^{(f)}$, and the data symbol $\boldsymbol{X}$ are also equal to 1.

Lets define the equivalent channel between the transmit vector x and y to be

$$\boldsymbol{J}_i = \sum_{p=1}^{P} A_{p,i} \boldsymbol{F}^H \boldsymbol{V}_{p,i} \boldsymbol{F} \boldsymbol{H}_p^{(f)}. \tag{3.33}$$

If the value of $a_{p,i}$ for all paths p is zero, the resulting channel is along the main diagonal as seen in Figure 3.2a. If instead the values of $a_{p,i}$ for the 5 paths are [0, -20, 10, -10, 20], the resulting channel consists of diagonals for each path off the diagonal.

The matrix $\boldsymbol{J}_i$ is shown in Figure 3.2 with and without the effect of Doppler shift.

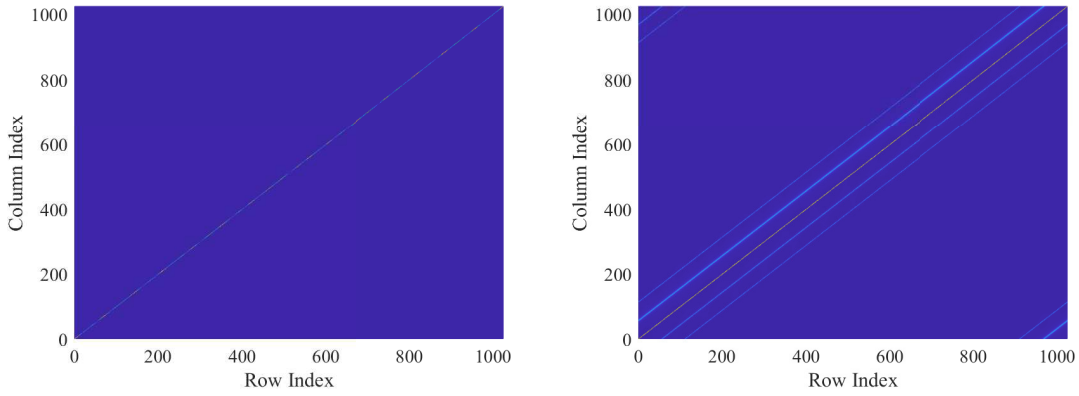

(a) Paths without Doppler Shift (b) Paths with Doppler Shift

Figure 3.2: Plots of $\boldsymbol{J}_i$ demonstrating the effect of time-variance on an OFDM symbol.

It can now be seen that while OFDM is a very spectrally efficient, it is highly susceptible to the Doppler effect which will result in Inter-Carrier Interference (ICI). To combat the effect of Doppler in the underwater channel, we now investigate Orthogonal Chirp Division Multiplexing (OCDM), which combines the multi-carrier modulation technique of OFDM with the chirp waveform (chirps have strong resilience to the effects of the underwater channel). The next section explains OCDM in detail. Though it is not within the scope of this thesis, future analysis work should include applying the Doppler shift model outlined in [19] to OCDM to compare the isolated effect of Doppler shift on both techniques.

3.3 Improving Multicarrier Performance with OCDM

Orthogonal Chirp Division Multiplexing [21], hereby referred to in this paper as OCDM, is another orthogonal multiplexing technique. Unlike OFDM, where a symbol is split into multiple frequency subcarriers, in OCDM a symbol is split into multiple chirp subcarriers. Each chirp is offset from the base chirp by a certain multiple of phase, so that the rate of change of frequency of each chirp is slightly different at a given point in time. These orthogonal chirps span the entire frequency band of the channel.

As explained in section 2, chirps have well documented use for military applications and underwater communication. The advantage of Chirp Spread-Spectrum (CSS) modulation is its resilience to the effects of the wireless communication channel (fading, Doppler, multipath). Chirps are excellent for low data rate applications where reliability of the communication link is the most important factor. OCDM attempts to combine the high throughput and spectral efficiency of OFDM with the reliability of CSS.

Let us now reconsider the chirp equation from Chapter 2, with its resilience to the effects of the UWAC channel:

$$\psi(t) = e^{j(\pi a t^2 + 2\pi\beta t + \varphi_0)} \tag{2.1}$$

The bandwidth of a chirp is proportional to its chirp rate a. The time-bandwidth product $B \times T$ is the chirp's processing gain. If more than one chirp exists in the same bandwidth and period, the two chirps will interfere with each other. Additionally, a chirp's time bandwidth product $B \times T >> 1$. Therefore, $B >> R_s$, where $R_s = 1/T$ is the chirp symbol rate. The spectral efficiency decreases with the processing gain.

In order to maximize the spectral efficiency, we require a series of orthogonal chirps (similar to the orthogonal frequency bands in OFDM). If we set the chirp rate $a = -(N/T^2)$ and each chirp is shifted with an integer multiple of $\Delta c = T/N$, we get a set of N orthogonal chirps without any inter-carrier interference (ICI).

For example, from [22], let $\psi_n(t)$ be a set of waveforms with chirp wave-number $n \in [1, N]$

$$\psi_n(t) = e^{j\pi/4} e^{-j(\pi N/T^2)(t-nT/N)^2}, 0 \leq t < T, \tag{3.34}$$

An example of a group of these waveforms can be seen in Figure 3.3.

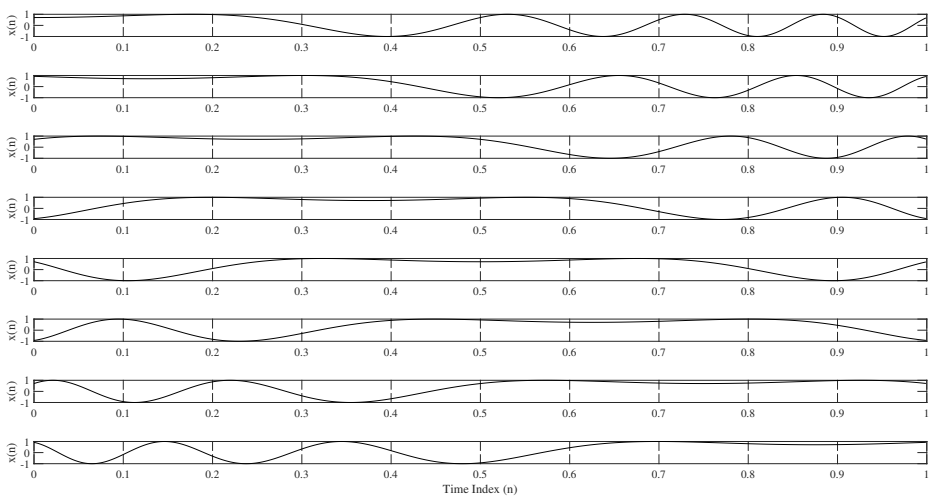

Figure 3.3: 8 Analog OCDM Waveforms with $N = 1$ to 8, from top to bottom.

Similar to OFDM before it, it can be proven that these chirp waveforms are orthogonal to each other from:

$$\int \psi_m^*(t)\psi_n(t)dt = \int_0^T e^{j\pi\frac{N}{T^2}(t-m\frac{T}{N})^2} e^{-j\pi\frac{N}{T^2}(t-n\frac{T}{N})^2} = \begin{cases} 1, & \text{if } n = m, \\ 0, & \text{otherwise.} \end{cases} \tag{3.35}$$

We can multiplex these N waveforms over a period T and multiply each waveform by a useful PSK or QAM symbol x_n^k to get an analog OCDM symbol $s_k(t)$:

$$s_k(t) = \sum_{n=0}^{N-1} x_n^k \psi_n(t), t \in [0, T]. \tag{3.36}$$

Just like with OFDM, it is possible to take advantage of the orthogonality property of OCDM to easily recover the received symbol $r_k(t)$ by using a matched filter at the receiver, and the transmit estimate is equal to

$$\hat{x}_k = \int_0^T r_k(t)\psi_n^*(t)dt. \tag{3.37}$$

To visualize the orthogonality, the output of a cross-correlation matched filter on an 8-subcarrier analog OCDM signal can be observed in Figure 3.4. It can be deduced that in a multi-path channel, there is a potential to lose orthogonality.

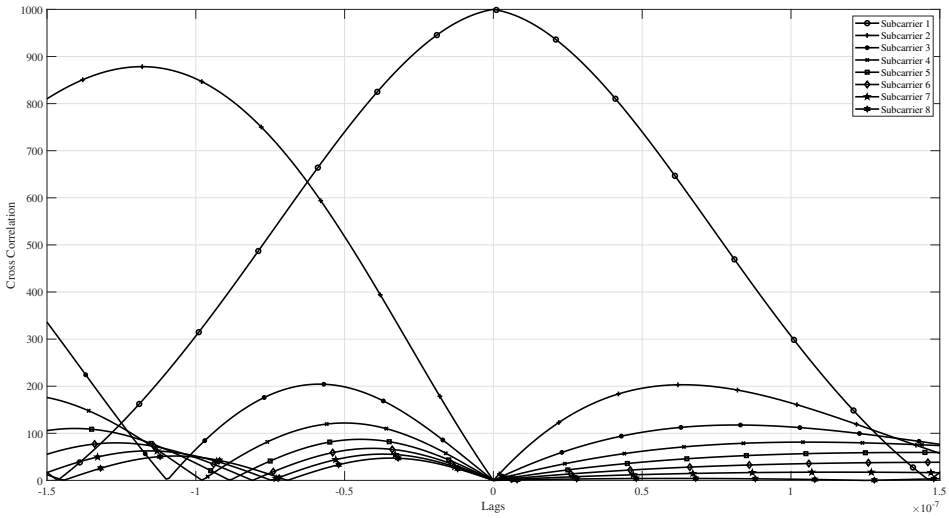

(a) Zoomed In

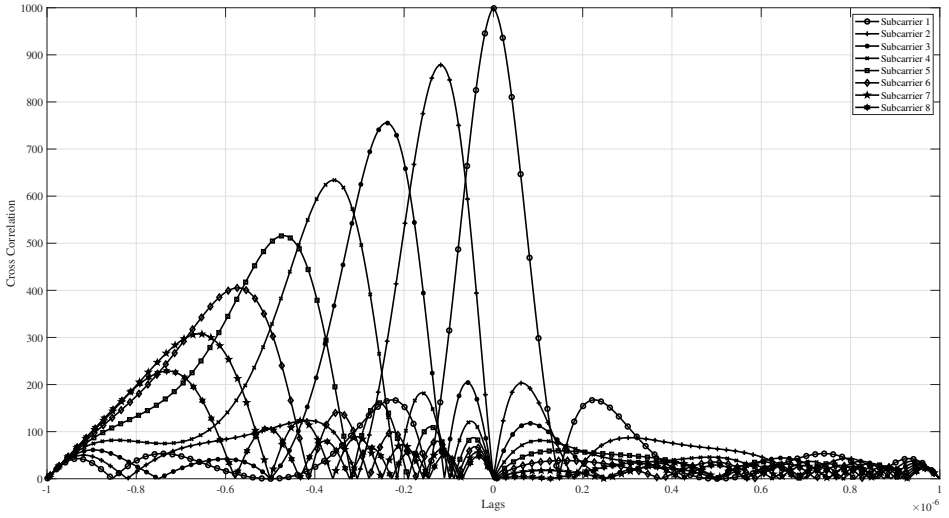

(b) Full view

Figure 3.4: Cross-correlation filter output of 8-channel analog OCDM

Equations (3.36) and (3.37) represent OCDM for analog signals. For digital signals, OCDM is enabled almost identically to OFDM. The one difference is that instead of using an FFT matrix $\boldsymbol{D}$, we use an Inverse Discrete Fresnel Transform (IDFnT)

matrix $\mathbf{\Phi}$.

The Fresnel integral transform comes from classical optics [21]. In $N \times N$ matrix form, the (m, n)-th entry of the discrete Fresnel transform (DFnT) matrix $\mathbf{\Phi}$ is

$$\mathbf{\Phi}(m,n) = \frac{1}{\sqrt{N}} e^{-j\frac{\pi}{4}} \times \begin{cases} e^{j\frac{\pi}{N}(m-n)^2}, & \text{if N is even} \\ e^{j\frac{\pi}{N}(m+1/2-n)^2}, & \text{if N is odd} \end{cases} \tag{3.38}$$

The DFnT of a circular convolution of two sequences is equal to either sequence convolving with the DFnT of the other sequence [23]. The entries of the DFnT matrix in (3.38) consist of the entries of the DFT matrix in (3.3) combined with the quadratic phase $\Theta_1(m)$:

$$\Theta_1(m) = e^{-j\frac{\pi}{4}} \times \begin{cases} e^{j\frac{\pi}{N}m^2}, & \text{if } N \text{ is even;} \\ e^{j\frac{\pi}{4N}} e^{j\frac{\pi}{N}(m^2+m)}, & \text{if } N \text{ is odd;} \end{cases} \tag{3.39}$$

as well as the quadratic phase $\Theta_2(n)$ defined as

$$\Theta_2(n) = \begin{cases} e^{j\frac{\pi}{N}n^2}, & \text{if N is even;} \\ e^{j\frac{\pi}{N}(n^2-n)}, & \text{if N is odd.} \end{cases} \tag{3.40}$$

Then, the DFnT can be implemented with a FFT in three steps:

1. multiply the transmit sequence by $\mathbf{\Theta_1}$;
2. perform the DFT using the FFT algorithm;
3. multiply by $\mathbf{\Theta_2}$;

where $\mathbf{\Theta_1}$ and $\mathbf{\Theta_2}$ are diagonal matrices whose m-th diagonal entries are $\Theta_1(m)$ and $\Theta_2(m)$, respectively. It is recommended that future works start with this procedure if implementing OCDM on a micro-controller or field-programmable gate array (FPGA) is desirable. The reasoning for this is to create a flexible underwater modem that can test the transmission of OCDM at low power and/or in real time, allowing it to achieve a small form-factor without needing to design a specific integrated circuit just for OCDM transmission.

Sampling (3.36) at a rate of mT/N gives

$$s_k[m] = s_k(t)_{t=m\frac{T}{N}} = \sum_{n=0}^{N-1} x_n^k \psi_n(mT/N) = e^{j\frac{\pi}{4}} \sum_{n=0}^{N-1} x_n^k e^{-j\frac{\pi}{N}(m-n)^2}. \tag{3.41}$$

From (3.41), the concise matrix form of OCDM modulation is expressed as

$$\boldsymbol{s}_k = \boldsymbol{\Phi}^H \boldsymbol{x}_k, \tag{3.42}$$

where $\boldsymbol{\Phi}^H$ is the Hermitian of the DFnT matrix for even integers of N from Eq. (3.38). To demodulate, we simply multiply $\boldsymbol{s}_k$ by $\boldsymbol{\Phi}$:

$$\hat{\boldsymbol{x}}_k = \boldsymbol{\Phi} \boldsymbol{s}_k. \tag{3.43}$$

The equalization of the received OCDM signal is described in greater detail in 4.1.3.

Now that OCDM and OFDM have been described in detail, the next chapter compares the reliability of the two techniques in simulation using channel data from St. Margaret's Bay and transmitter data from Ultra Maritime. Both OFDM and OCDM are then transmitted in the Dalhousie Aquatron, equalization techniques are described and the results are analyzed.

Chapter 4

Performance Analysis

In this chapter, the communication link reliability for OFDM and OCDM are compared. First, in Section 4.1, the BER of OCDM is compared to OFDM using channel impulse responses taken during a sea trial run 10-km off the coast of Nova Scotia, near St. Margaret's Bay. Next, in Section 4.2, the effect of the transmitter front-end frequency response is investigated. Finally, Section 4.3 compares the two modulation techniques for a high-throughput link established at a frequency of 27 kHz and tested in seawater tanks.

4.1 Simulation using St. Margaret's Bay Channel Data

The objective of this section, is to assess the performance of OCDM and compare its reliability to that of OFDM in realistic conditions for a long-range communication link. For this purpose, first, in Section 4.1.1, the simulation conditions that represent a realistic long-range environment are described; then, in Section 4.1.2, the performance of OFDM is provided, followed by Section 4.1.3, that describes the performance of OCDM; then, in Section 4.1.4, the two modulation techniques are compared.

4.1.1 Simulation Conditions

To properly compare OCDM to OFDM, first a simulation was performed in MATLAB. To create the transmit symbol:

1. A pseudo-random BPSK sequence is generated.
2. A discrete OFDM or OCDM symbol is created by modulating this BPSK sequence using the appropriate transforms for OFDM or OCDM (Fourier or Fresnel).
3. A cyclic prefix with a length equal to 1/4 the length of the OFDM or OCDM symbol is added to the beginning of the OCDM or OFDM symbol.

4. The discrete symbol with cyclic prefix is upsampled at the oversampling ratio.

5. The upsampled symbol is passed through a root-raised-cosine filter with a roll-off factor of 0.25.

6. The transmit symbol is upconverted to passband. This greatly increases simulation time but allows to modeling of real transmit conditions.

The transmit symbols contained 512 subcarriers. One symbol was transmitted repeatedly for each of OFDM and OCDM: the symbol does not change during the simulation. The simulation was stopped when either 200 total bit errors had occurred, or 200,000 symbols were transmitted. 200 bit errors is the confidence interval, determined by trial & error on a BPSK-OCDM symbol, that allows for a sufficient number of errors to plot smooth curves. BPSK in an AWGN channel was simulated first and compared to the theoretical BER of BPSK to confirm that the OCDM and OFDM algorithms were implemented correctly. Statistical variations in other channel models may indicate that a higher number of errors would be more appropriate in future simulations. The individual OCDM and OFDM simulations are detailed in Section 4.1.2 and Section 4.1.3. Symbols were transmitted across a channel constructed from data obtained in the DALCOMM1 experiment near St. Margaret's Bay, 10 km off the coast of Halifax, Nova Scotia. A picture of the time-varying channel impulse response is shown in Figure 4.1.

DALCOMM1 was run in the Summer 2016 to demonstrate the communication reliability for a range as long as 10 km. The objective of the experiment was to test different modulation techniques are different ranges up to 10 km and to estimate the channel for the different ranges. The carrier frequency chosen for this application was approximately 2048 Hz and the 3-dB bandwidth of the transmitter sound source limited the transmit symbol rate. The channel data used for this simulation is sourced from Receiver 5 of the DALCOMM1 experiment. This receiver was placed at a distance of roughly 10 km away from the transmit source.

The simulation was carried out under numerous oversampling ratios (relative to the underloading ratios, bandwidths, bitrates, and symbol rates, which are summarized in Table 4.1. These parameters are the same for both OFDM and OCDM.

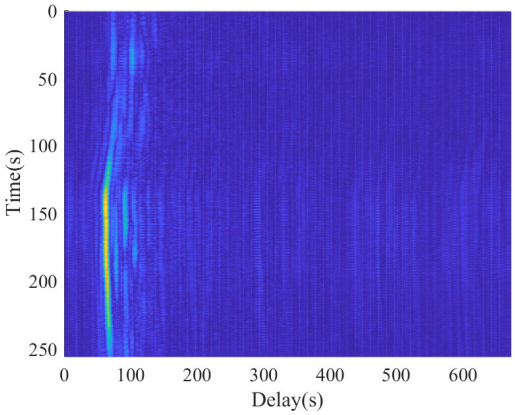

Figure 4.1: St. Margaret's Bay Channel Rx 5 during DALCOMM1 experiment

Table 4.1: OFDM/OCDM Simulation Transmission Properties

Oversampling Ratio	42	21	14	10
Underload Ratio	Bit Rate (bits/sec)			
1	236	458	668	905
2	118	229	334	452
4	59	114	167	226
8	29	57	83	113
Signal Bandwidth (Hz)	243.8	487.6	731.4	1024
Symbol Rate (syms/sec)	0.4618	0.8964	1.306	1.769
Sampling Frequency (Hz)	10240			
Carrier Center Frequency (Hz)	2048			
Number of Subcarriers N	512			
Number of Symbols Transmitted	Up to 200 000			

The bandwidth and symbol rate of transmission are dependent on the oversampling ratio: the more oversampled the signal is, the slower the symbol rate and the less bandwidth a symbol occupies. The symbol rate in Table 4.1 is that of the OCDM or OFDM symbol with the addition of a cyclic prefix. The bit rate is determined by both the oversampling ratio, as well as the underloading ratio. The underloading ratio represents the number of subcarriers with useful data vs the number of subcarriers with "holes" (they carry no data). For example, an underload ratio of 4 indicates that there is useful information only on every 4th subcarrier.

4.1.2 OFDM Performance

The communication link modelled is described by Figure 4.2.

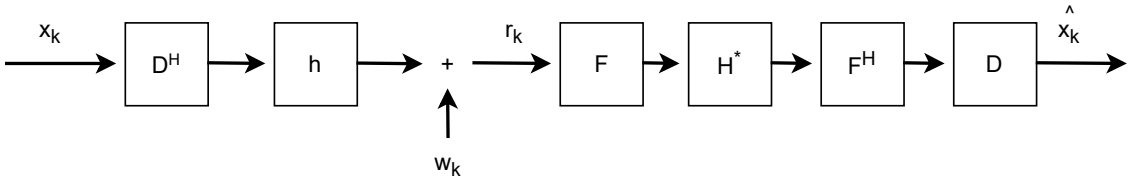

Figure 4.2: Simple OFDM Equalizer

First, a pseudo-random BPSK sequence $\boldsymbol{x}_k$ is generated. $\boldsymbol{x}_k$ is multiplied by $\boldsymbol{D}^H$, which is an N by N matrix representation of the Inverse Discrete Fourier Transform (IDFT) to produce the transmit symbol. A cyclic prefix of length L (where L is the length of the channel impulse response $\boldsymbol{h}$) is added to this transmit symbol to provide a guard interval and improve multipath performance. The OFDM symbol is upsampled, and then passed across a root-raised-cosine filter with a roll-off factor of 0.25. This filtered signal is then upconverted to passband. The passband has a centre frequency of 2048 Hz. Upconverting to passband is done during this part of simulation in preparation for testing in real bodies of water with a real transmitter. The transmit symbol is passed along the representation of the channel $\boldsymbol{h}$, and random noise $\boldsymbol{w}_k$ is added. This produces the received symbol $\boldsymbol{r}_k$, which is downconverted back to baseband and then filtered to remove imaging. $\boldsymbol{r}_k$ is then downsampled and the cyclic prefix is removed. The received symbol is then passed through a very simple equalizer. $\boldsymbol{r}_k$ is converted to the frequency domain via Fast Fourier Transform

(FFT). This frequency-domain symbol is combined with a frequency-domain complex-conjugate representation of $\boldsymbol{h}$, $\boldsymbol{H}^*$, to counteract the effects of the channel. An IFFT is performed on the received symbol, and then multiplied by the Discrete Fourier Transform matrix $\boldsymbol{D}$ to recover $\boldsymbol{x}_k$.

OFDM symbols were transmitted in simulation until a total of 200 bit errors were detected, up to a maximum of 200,000 OFDM symbols for each SNR, and the probability of bit error was examined as a function of signal to noise ratio (SNR). The results of these simulations are graphically represented in Figure 4.3.

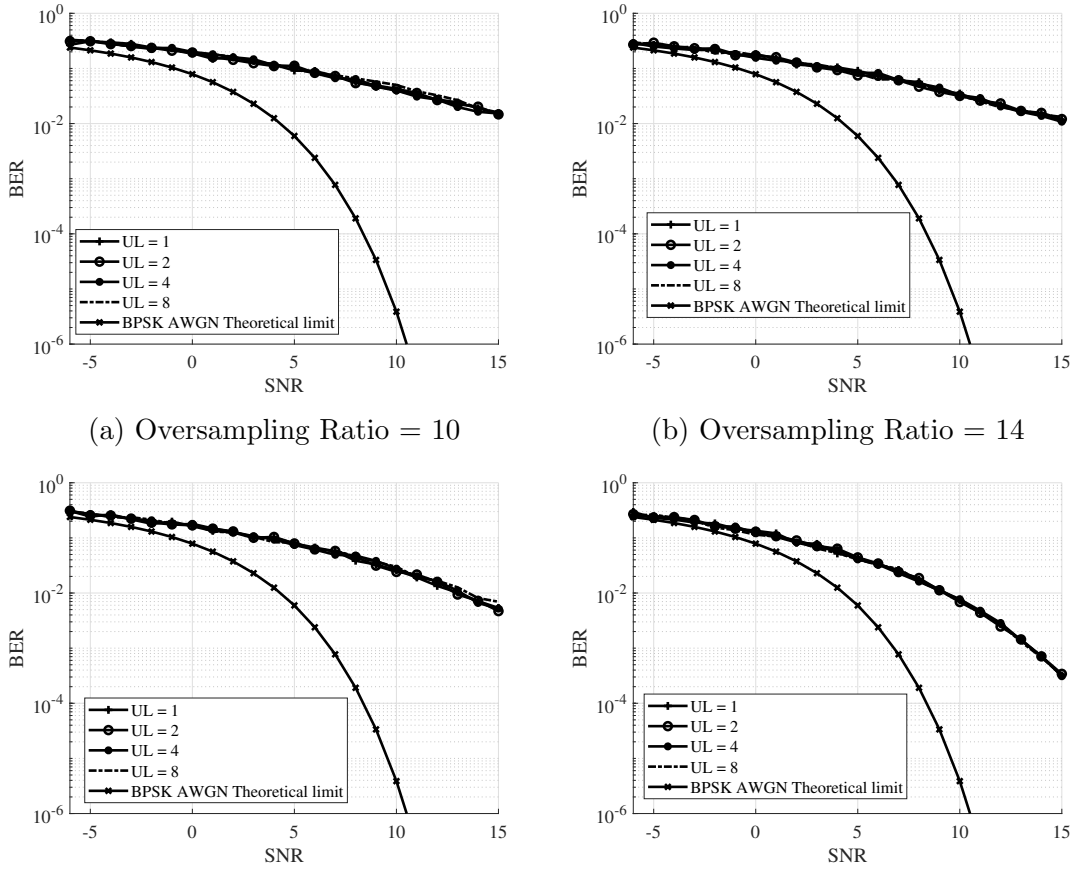

(a) Oversampling Ratio = 10

(b) Oversampling Ratio = 14

(c) Oversampling Ratio = 21

(d) Oversampling Ratio = 42

Figure 4.3: Performance of OFDM in static channel conditions at various oversampling and underloading ratios.

From Figure 4.3, it can be seen that as you increase the oversampling ratio (therefore decreasing the transmission rate), you increase the reliability and reduce the bit error rate (BER). Altering the underloading ratio does not seem at first inspection

to have an impact on error rates. The next section of this chapter details the same simulations but using OCDM instead of OFDM.

4.1.3 OCDM performance

For OCDM, a similar procedure is followed as for OFDM. The main difference before transmission is that instead of using a matrix $\boldsymbol{D}$ to represent the Discrete Fourier Transform, we use a diagonal N x N matrix $\boldsymbol{\Gamma}$ to represent the Discrete Fresnel Transform (DFnT). Additionally, for OCDM, a more complex equalizer is implemented as in [22]. A graphical representation of this MMSE equalizer is shown in Figure 4.4

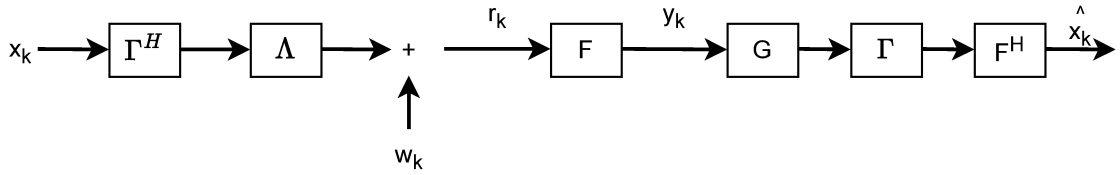

Figure 4.4: OCDM MMSE Equalizer

In Figure 4.4, x_k is the transmitted symbol after adding filtering and a cyclic prefix, $\boldsymbol{w}_k$ is a gaussian noise vector with zero mean and variance noted σ_ω^2. $\boldsymbol{\Gamma}^H$ is a diagonal matrix of size $N \times N$. In this case, with N being even, it is equal to

$$\boldsymbol{\Gamma}^H = e^{-j(\pi/N)n^2}, \tag{4.1}$$

where $\boldsymbol{\Gamma}$ accounts for the phase rotation caused by the DFnT. $\boldsymbol{\Lambda}$ is a diagonal matrix of size $N \times N$, in which the element at position (n, n) is defined as

$$\boldsymbol{\Lambda}(n, n) = \boldsymbol{H}(n, n), \tag{4.2}$$

where $\boldsymbol{H}(n, n)$ is the channel frequency response of the channel at the n-th frequency bin. $\boldsymbol{H}(n, n)$ can be obtained by channel sounding. The $\boldsymbol{H}(n, n)$ used in this simulation is measured data from St. Margarets Bay.

Once the transmit symbol has passed through the channel, the received symbol $\boldsymbol{r}_k$ is multiplied by $\boldsymbol{F}$, an $N \times N$ matrix representation of the Fourier Transform. It follows that

$$\boldsymbol{y}_k = \boldsymbol{F}\boldsymbol{r}_k = \boldsymbol{\Gamma}^H \boldsymbol{\Lambda} \boldsymbol{F} \boldsymbol{x}_k + \boldsymbol{w}_k, \tag{4.3}$$

$\boldsymbol{y}_k$ is then multiplied by $\boldsymbol{\Lambda}$, and that result is multiplied by $\boldsymbol{G}$. $\boldsymbol{G}$ is a diagonal equalization matrix optimized under Minimum Mean Square Error (MMSE) criterion

such that:

$$\boldsymbol{G} = \boldsymbol{\Lambda}^H(\boldsymbol{\Lambda}^H\boldsymbol{\Lambda} + \sigma_\omega^2\boldsymbol{I})^{-1}, \tag{4.4}$$

where $\boldsymbol{I}$ is an $N \times N$ identity matrix. Similarly to OFDM, 200,000 OCDM symbols were transmitted in simulation. The resulting BER vs SNR plots are detailed in Figure 4.5

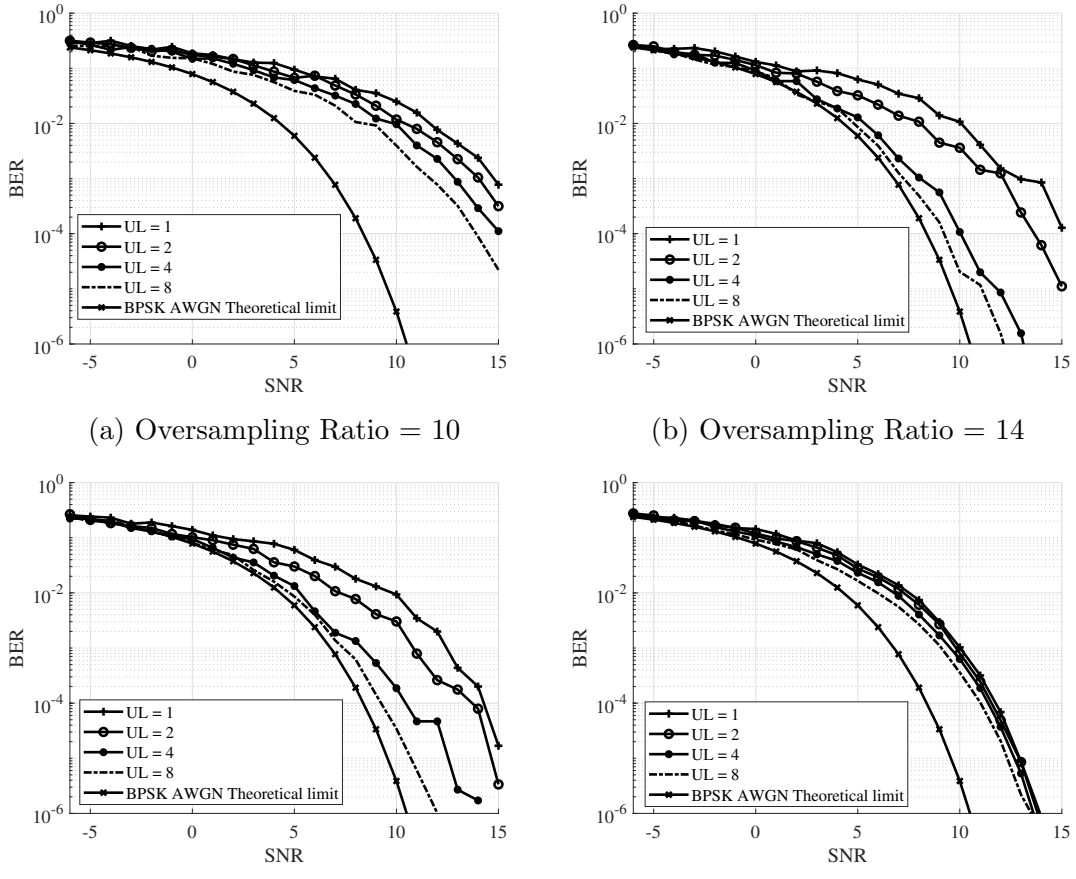

(a) Oversampling Ratio = 10

(b) Oversampling Ratio = 14

(c) Oversampling Ratio = 21

(d) Oversampling Ratio = 42

Figure 4.5: Performance of OCDM in static channel conditions at various oversampling and underloading ratios.

Compared to OFDM, OCDM at first glance provides much lower errors as the underload ratio is increased: the more empty subcarriers that are transmitted, the better the error rate. This was not the case for OFDM.

4.1.4 Comparison of OCDM to OFDM

Having performed simulations on both OFDM and OCDM, the two techniques are directly compared in terms of BER vs SNR in Figure 4.6

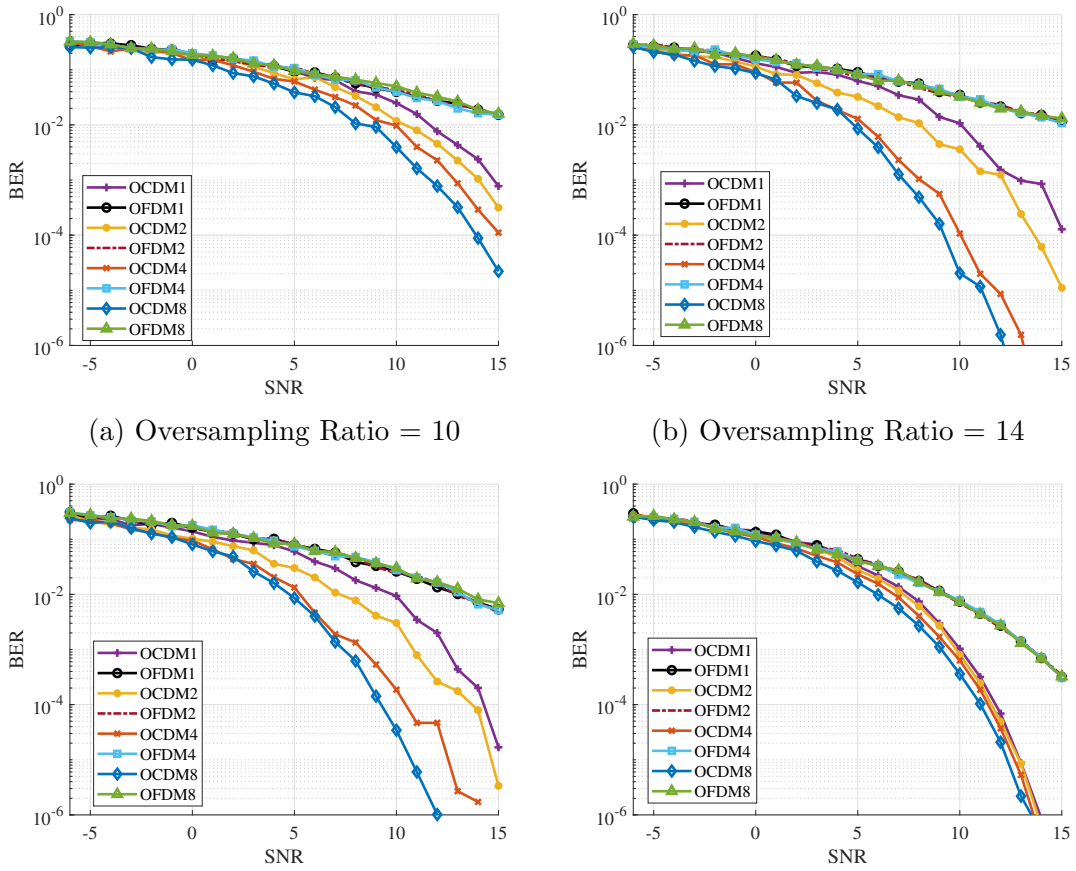

(a) Oversampling Ratio = 10

(b) Oversampling Ratio = 14

(c) Oversampling Ratio = 21

(d) Oversampling Ratio = 42

Figure 4.6: Performance of OCDM vs OFDM in static channel conditions at various oversampling and underloading ratios. The number in the legend indicates underload ratio.

In general, from this simulation it can be observed that OCDM outperforms OFDM in a static multipath channel. This is especially true for higher underload ratios: adding more empty subcarriers can dramatically improve performance of OCDM compared to OFDM, at the cost of bit rates. A trade-off between throughput and reliability must be considered when determining the oversampling and underloading ratios.

Next, pre-equalization at the transmitter is investigated to improve the link reliability by compensating for the effect of the transmitter frequency response.

4.2 Effect of Transmitter Frequency Response

Pre-equalization

The last step in a transmitter chain, and the first step in a receiver chain, is a transducer: a device that turns electrical energy into mechanical energy and vice-versa. The receiver transducers used in this thesis have a frequency response that is approximately flat between 10 Hz and 200 kHz. This is not the same for the transmitter transducer: it has a more narrow resonant frequency which reduces its usefulness in bands outside of this resonant frequency. The resonant frequency of the transducer tested in these simulations is 2048 kHz. This resonant frequency is a physical property of the transducer and cannot be easily changed, and reduces the possible bandwidth of the transducer.

To try to get around this problem, equalization can be done pre-transmission. In this thesis, a zero-forcing pre-equalizer [24] is implemented at the transmitter to get the transducer response to act as a brickwall filter preventing frequency selective distortion. The pre-equalizer effectively increases the bandwidth of the transmitter and therefore allows signals with increased throughout.

Impact of the front-end frequency response

Underwater acoustic signal transmission requires the use of an acoustic projector to generate the acoustic pressure waves. An acoustic projector is a mechanical transducer, typically made of ceramics, that vibrates at a certain acoustic frequency when a voltage is applied across the transducer. A given transducer is typically designed to resonate at a certain frequency. The measured properties of the transducer being tested in this section were provided by Ultra Electronics Maritime Systems. The range of frequencies for which a transducer can operate at can be shown in the transducer transmit voltage response (TVR) curve, as seen in Figure 4.7a.

The TVR curve of the example transducer in Figure 4.7a demonstrates that the

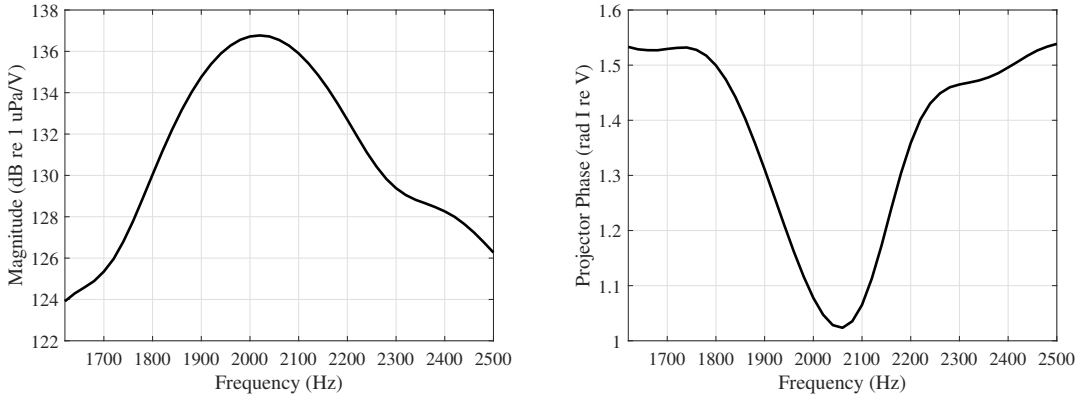

(a) Transducer TVR Curve (b) Transducer Phase-Frequency Curve

Figure 4.7: Measured properties of a transducer used for the purposes of simulation.

transducer itself acts on the signal in a similar manner to a frequency selective channel because the transducer frequency response is not frequency flat. This frequency selectivity of the transducer causes an undesirable loss of power and reduction in total useful bandwidth outside of the 3dB drop off range.

To compensate for the frequency selectivity of the transducer, a zero-forcing equalizer is constructed from the measured frequency and phase curves given in Figure 4.7 and inserted in the communication link directly ahead of the transducer. The TVR curve by itself only provides frequency and amplitude, but does not provide phase, so the phase at each measured frequency must be provided as seen in Figure 4.7b.

The concept of a zero-forcing equalizer is very simple. First, the single sided frequency response of the transducer $X_{Tdr}(f)$ is obtained by combining the measured frequency and phase data:

$$X_{Tdr}(f) = 10^{\mathrm{TVR}/20} e^{j\phi}, \tag{4.5}$$

where the TVR is the measured amplitude of the TVR curve in dB and ϕ is the measured phase. Next, $X_{TDR}(f)$ is mirrored about the frequency axis to produce a double-sided transducer frequency response shown in Figure 4.8a.

Afterwards, the double-sided frequency response is converted back to the time domain via IFFT and then passed through a low-pass filter to remove the frequencies that we are not interested in (which in this case are any frequencies outside the point

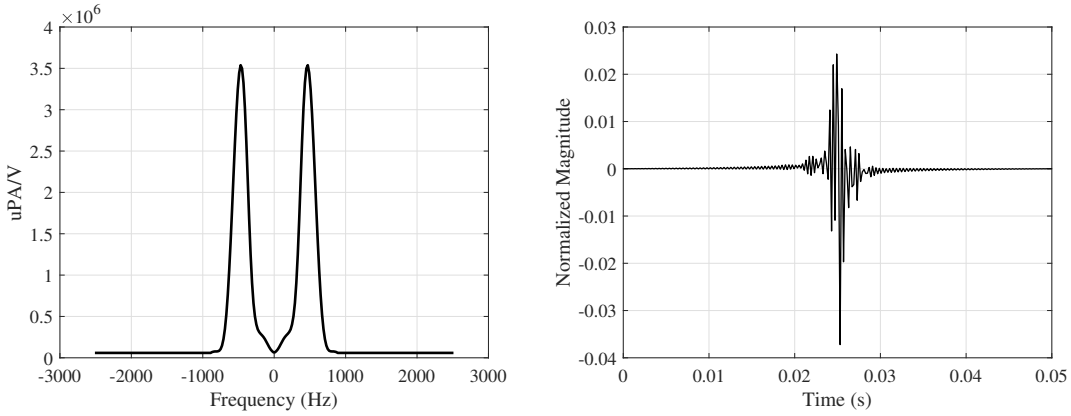

(a) Frequency response (b) Impulse Response

Figure 4.8: Double sided response of the transducer with measured properties from 4.7

where our response drops by 3dB or more). After filtering, our response is resampled to match the sampling frequency of our transmit waveform. All of this gives us our time-domain transducer impulse response $x_{TIR}(t)$.

Now, to implement the zero-forcing equalizer, $x_{TIR}(t)$ is converted back to the frequency domain via FFT. The zero-forcing equalizer is produced by inverting this processed transducer frequency response:

$$Z[f] = 1/X_{TIR}[f]. \tag{4.6}$$

When multiplied together in the frequency domain, the two cascaded filters in the signal band can be represented using a transfer function equal to

$$Z[f]X_{TIR}[f] = 1, \tag{4.7}$$

which produces a flat response for the overall frequency response of the cascaded systems. If converted back into the time domain via IFFT, the convolution of $x_{TIR}(t)$ and $z(t)$ produces a single impulse response centered around the midway point between $x_{TIR}(t)$ and $z(t)$. This results in a pulse that is less spread in time. This process is graphically demonstrated in Figure 4.9.

Compensating for the frequency selectivity of the transducer has the added benefit of removing the "skirts" of the transducer response, effectively increasing the transmission bandwidth. In our example, the 3-dB bandwidth of the transducer is 320 Hz.

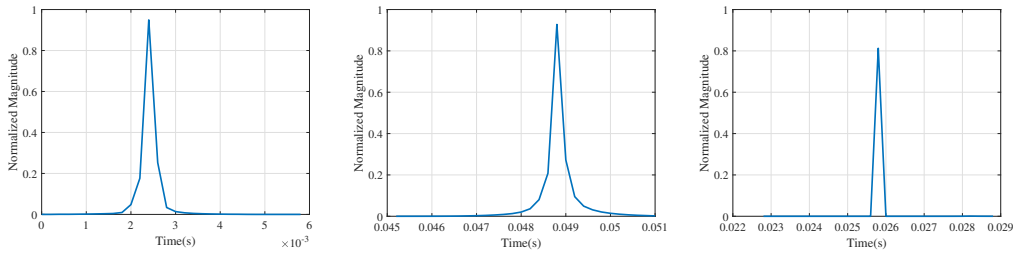

(a) $x_{TIR}(t)$ (b) $z(t)$ (c) $x_{TIR}(t) \circledast z(t)$

Figure 4.9: Close up diagram of the zero-forcing pre-equalizer impulse response showing the reduced width of the TIR after convolution

After compensation, this bandwidth is expanded to 400 Hz, for a 25 percent increase in bandwidth. This lines up with the roll off factor of 0.25 that is used in our cosine filter to smooth out the signal as it is oversampled and upconverted to passband.

The pre-equalizer was tested by transmitting 10,000 symbols across 3 different time-invariant channels: AWGN, a simple multipath channel, and a slice of channel data taken from St. Margaret's Bay in Halifax, Nova Scotia. The channel impulse responses can be seen in Figure 4.10.

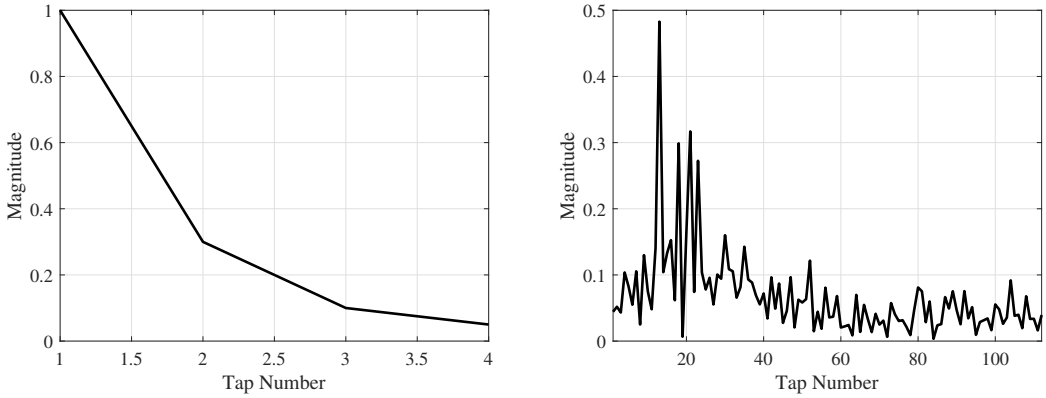

(a) Simple Multipath Channel (b) St. Margaret's Bay

Figure 4.10: Impulse responses of the different channels being tested. The AWGN channel is omitted from the figure. Magnitude of the response at each tap is normalized

The simulation was run using 512-OCDM with an oversampling ratio of 42 and an underloading ratio of 1. At the receiver, the MMSE equalizer from Figure 4.4

is incorporated. The simulation was performed over three scenarios: no transducer or zero-forcing pre-equalizer, a transducer but no zero-forcing pre-equalizer, and a transducer and a zero-forcing pre-equalizer. The results are shown in Figure 4.11.

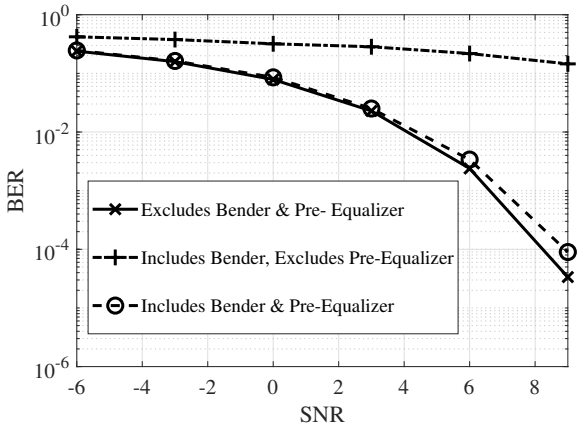

(a) AWGN Channel

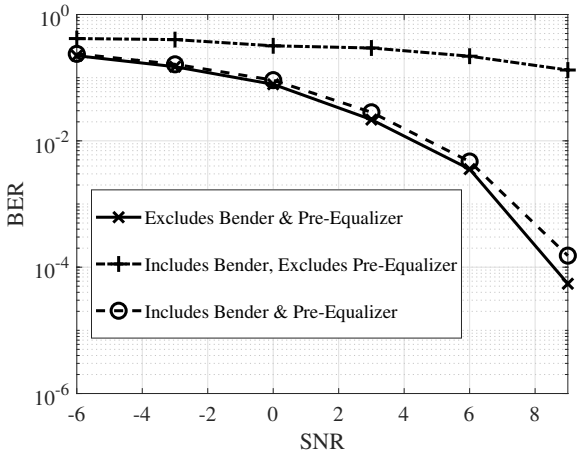

(b) Simple Multi-path Channel

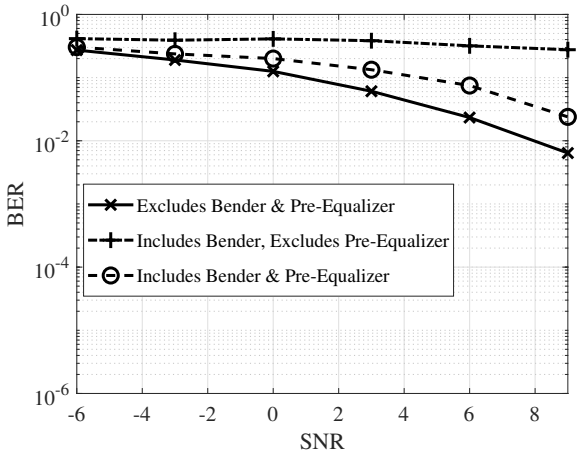

(c) DALCOMM1 Channel

Figure 4.11: Performance impact of zero-forcing equalizer to compensate for frequency selectivity of acoustic transducer.

From Figure 4.11, it can be seen that for OCDM, without the use of a zero-forcing pre-equalizer to compensate for the effect of the transducer, performance in terms of BER vs SNR degrades significantly. One assumption for this is that the receiver MMSE equalizer is built using pre-existing channel data but does not account for the effect of the transducer, so the receiver is incomplete on its own. Doing equalization at the transmitter first before reception means that the transmitter and receiver can be decoupled from each other: a receiver is free to do its own channel sounding and measurement independent of any given transmitter, and more importantly in the absence of noise.

After running all of these simulations, it is important to test the performance of these techniques in a real environment. What follows is a description of an experiment that took place in the Dalhousie Aquatron.

4.3 Comparison of the Performance for a Link at 27.5 kHz

An experiment was performed in the Dalhousie Aquatron in May 2021 to assess the performance of OCDM at a carrier frequency of 27.5 kHz: this experiment was originally intended to be performed at 2 kHz using the transducer provided in Section 4.2 in an open-water environment, but that experiment was cancelled due to the COVID-19 global pandemic. Instead, this experiment serves as a complementary data set to the simulations in the previous sections.

A total of 24 different waveforms were transmitted: OCDM with underload ratios of 1, 2, 4, and 8, and OFDM with underload ratios of 1, 2, 4, and 8. Each waveform group was transmitted with 256 subcarriers, 64 subcarriers, and 16 subcarriers.

The Dalhousie Aquatron is a static tank that has a volume of approximately 271 cubic metres, and is 9.10 m long, 7.10 m wide, and 4.25 m deep. The dimensions of the tank are illustrated in Figure 4.12.

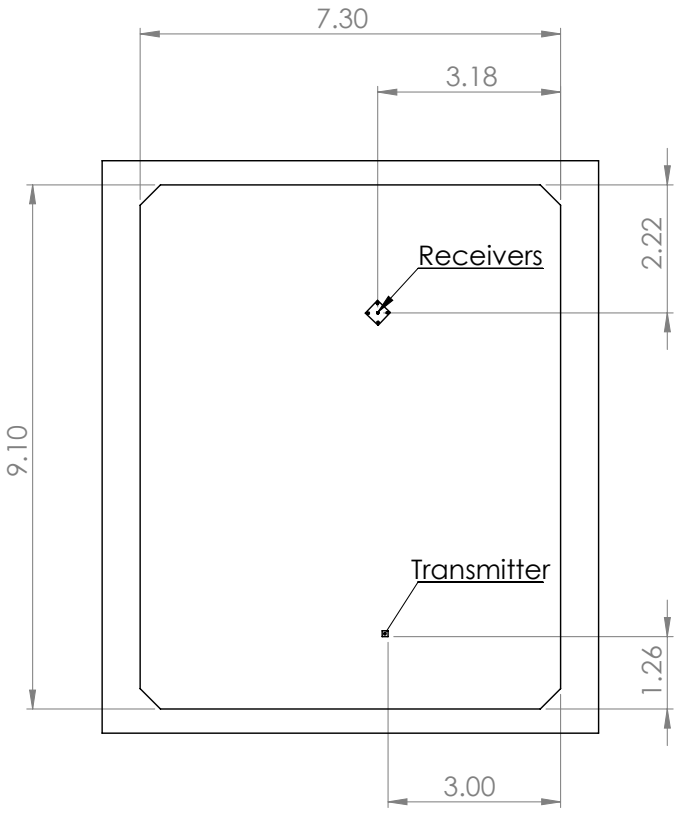

(a) Top view

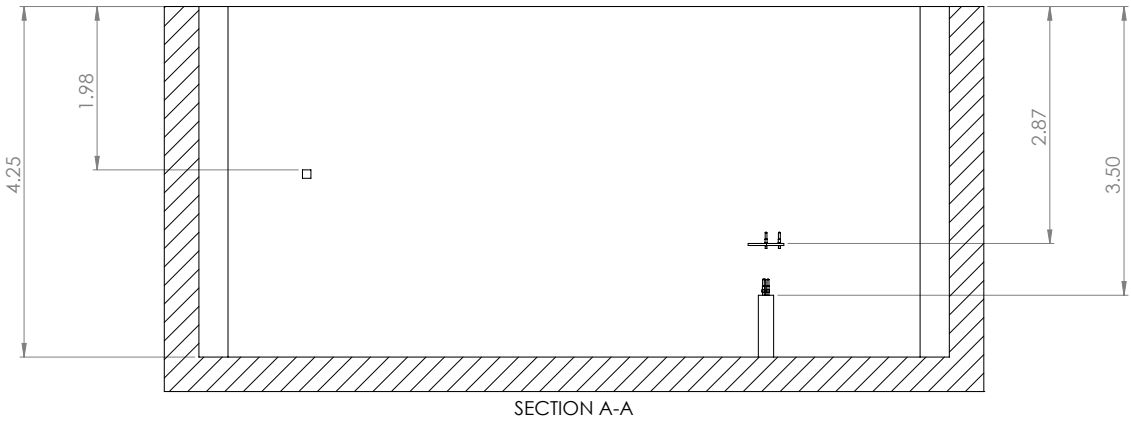

(b) Section view

Figure 4.12: Dalhousie Aquatron dimensions.

The transmitter was a Benthowave BII-7522 omnidirectional projector with a centre frequency of 27.5 kHz, driven by a BII-5021 power amplifier. The projector was suspended in the centre of the tank, approximately 1 m below the surface. The receiver, consisting of 5 Geospectrum hydrophones arranged in a cross pattern, rests on the bottom of the tank. These can be seen in Figure 4.13. The transmitters in 4.13a were connected to a Rigol function generator (not pictured) as opposed to the computer shown in this figure. The transmitter was suspended in the water, hanging from the platform in Figure 4.13b. The receiver rests on the bottom of the tank in 2 parts: the majority of the hardware sits on the bottom of the tank in the pressure case in Figure 4.13c, and the 5 hydrophones are suspended above the pressure case by a buoy, arranged in a cross pattern (Figure 4.13d)

The waveforms were developed in MATLAB R2019b and then saved to a flash drive and ported to a Rigol DG4162 function generator. There was a limitation to this function generator: the waveforms produced by the generator could only have up to 16384 sample points. For the purposes of waveform resolution, this limited the transmissions to a maximum of 256 subcarriers. It also required generating the signals at difficult sampling frequencies and oversampling ratios. Table 4.2 details the properties of the signals as they were transmitted.

Table 4.2: Properties of the OCDM and OFDM Symbols Transmitted in the Aquatron, May 2021

# of Subcarriers	Oversampling Ratio	Sampling Freq (Hz)	Fn Gen Freq (Hz)
256	50	163,840	10
64	200	655,360	40
16	800	2,621,440	160

These properties were required to achieve transmit symbols with 12800 sample points. Another 3200 points were added via a cyclic prefix 1/4 the size of the transmit symbol, and finally a guard band of 384 points was added to arrive at the full number of 16384 sample points. This produced a symbol that took 99.7ms to transmit: Table 4.3 shows the exact time of each portion of the full transmit symbol, and Table 4.4 shows the bit rates of each transmitted signal:

A roughly calculated Aquatron channel was simulated using the geography of the

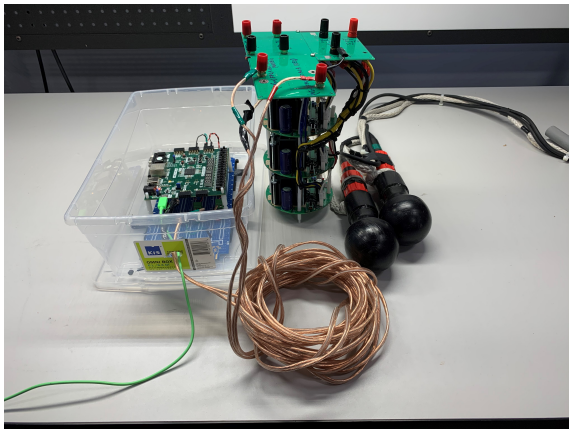

(a) Transmitter Hardware

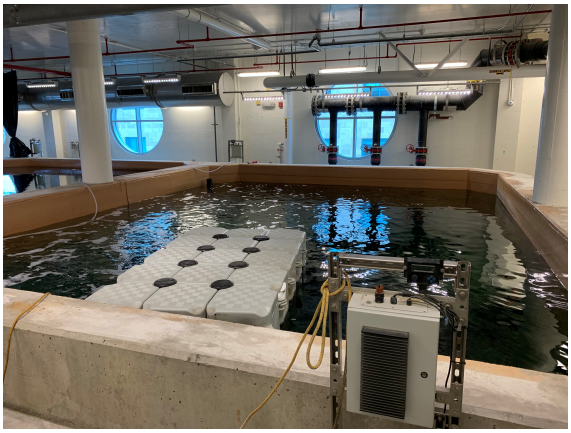

(b) The Aquatron Tank

(c) Receiver Pressure Case

(d) Receiver Hydrophones

Figure 4.13: Hardware used in the May 2021 Aquatron Experiment.

Table 4.3: Length of Time of Each Portion of the Transmitted Symbols in Milliseconds

OCDM/OFDM	Cyclic Prefix	Guard Band	Total
77.9	19.5	2.3	99.7

Table 4.4: Bit Rate of Transmit Signals (Rounded Down)

Underload Ratio	1	2	4	8
# of Subcarriers	Bit Rate (bits/sec)			
256	2567	1283	641	320
64	641	320	160	80
16	160	80	40	20

tank. Four arrival paths were measured: direct line of sight, one bounce from the top of the tank to the receiver, one bounce from the bottom of the tank to the receiver, and two bounces (one from the top of the tank to the back wall, then from the wall to the receiver). Path arrival times were calculated using these measured distances and the speed of sound in water. The mean value of these 4 arrival times was calculated and then used to generate 50 path arrivals. The intensity of each path is relative to the direct line of sight path, which is set equal to 1. This produced the channel shown in Figure 4.14:

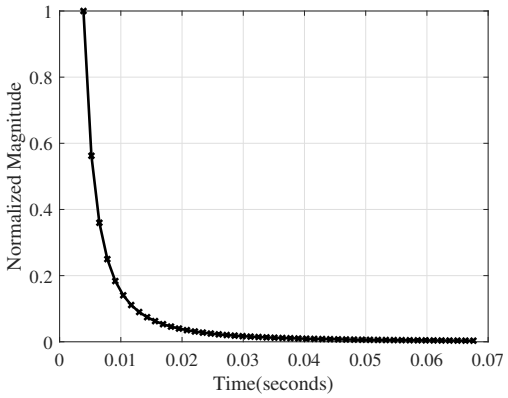

Figure 4.14: Calculated Aquatron Channel

In simulation, 10 OFDM symbols were then transmitted across the channel shown in Figure 4.14. An estimate of the channel was then calculated by taking a cross-correlation of one of these received symbols and convolving it with an OFDM symbol (excluding cyclic prefix and guard band). Common practice would be to use the cyclic prefix for channel estimation, but the cyclic prefix in this case is too short: the limitations of the function generator resolution prevented a sufficiently sized CP from being appended to the transmit symbol. There is still appreciable energy outside the

CP time, so the full OFDM symbol is used instead. The channel estimate compared to the calculated channel is shown in Figure 4.15.

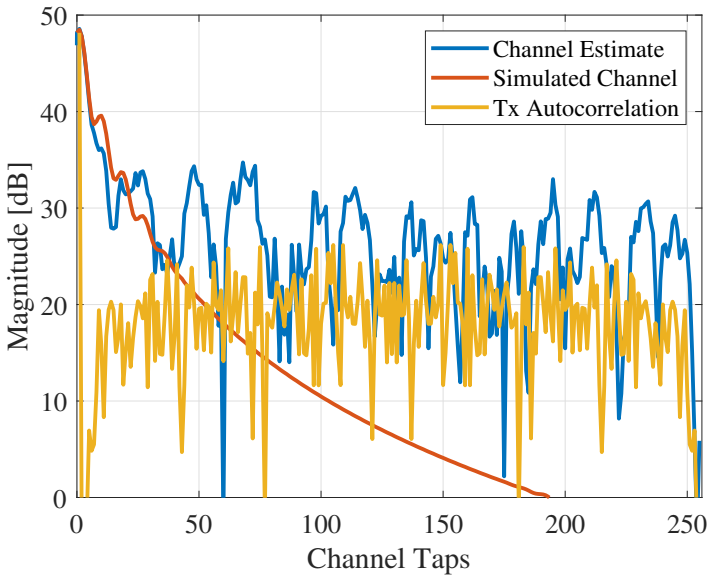

Figure 4.15: Calculated Aquatron Channel vs Aquatron Channel Estimate

From Figure 4.15, it can be seen that the transmit symbol is very noisy. The same simulation was performed with OCDM and the transmit symbol was similarly noisy.

During the live experiment in the Aquatron, the received data was saved as .WAV files and downloaded from the receiver, then imported to MATLAB 2019b.

The same equalization technique, outlined in Figure 4.2, is used for both OCDM and OFDM recovered symbols, with the major difference being that OCDM uses the $\boldsymbol{\Phi}$ matrix outlined in Section 3.3 instead of the $\boldsymbol{D}$ matrix used in Figure 4.2. The MMSE equalizer used in simulation is not used in the Aquatron experiment. An estimate of the Aquatron channel using real OFDM data can be seen in Figure 4.16. This channel is nearly identical to the channel estimated using OCDM, and so only one figure is shown.

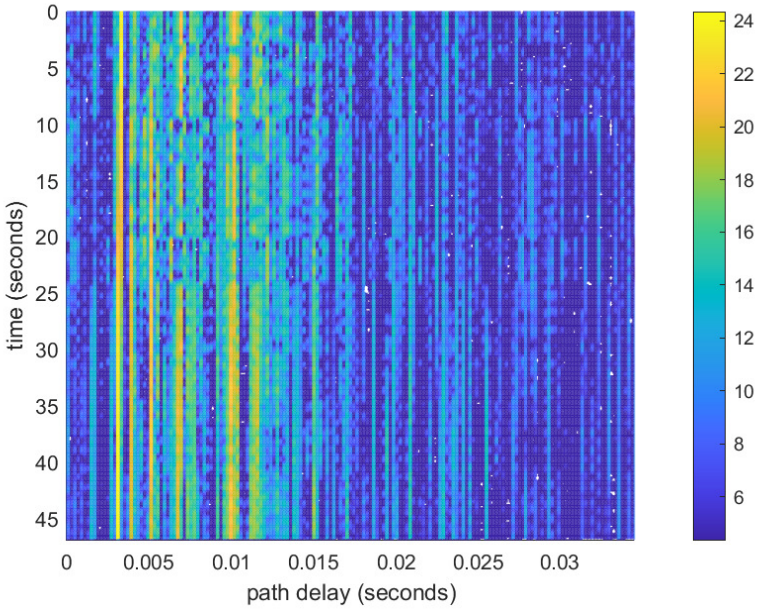

Figure 4.16: Aquatron Channel Estimate Spectrogram

This channel matches the simulation channel data: there is a very strong and clear first path response, followed by a lot of multipath. There are discontinuities in the channel, such as around seconds 3, 10, and and 22, where it is possible that relative motion between the transmitter and the receiver impacted the path delays. Another source of these discontinuities could be clock drift: there is a difference in clock speed between the transmitter and the receiver. In post-processing, the received data was resampled at a ratio of 5003/5000, but this may not be the most accurate resolution.

24 different permutations of signal were transmitted: 12 OFDM and 12 OCDM. Each permutation was transmitted for roughly 40 seconds, with roughly 420 symbols transmitted per permutation. Symbols were recovered 4 symbols at a time: the first symbol in each group of 4 was used as the training symbol, and the following 3 symbols were compared against this training symbol. Attempting to use the training symbol on received symbols that were 4 or more symbols away in time introduced a dramatic drop in performance (most of them were unrecoverable). This could be explained by the large amounts of multipath leading to inter-symbol interference in the small confined space of the Aquatron. The bit error rates for each signal permutation are compared in Table 4.5.

Table 4.5: Comparison of OCDM and OFDM BERs for Aquatron Experiment

256 Subcarriers		
Underload Ratio	OCDM BER	OFDM BER
1	0.0037	0.0334
2	0.0020	0.0069
4	0.0058	0.0058
8	0.0029	0.0085
64 Subcarriers		
Underload Ratio	OCDM BER	OFDM BER
1	9.8630e-04	0.0019
2	0	0.0014
4	0	0
8	4.1528e-4	0
16 Subcarriers		
Underload Ratio	OCDM BER	OFDM BER
1	0.0302	0.0297
2	0.0279	0.0212
4	0.0058	0.0232
8	0.0116	0.0041

Studying Table 4.5 more closely leads to some conclusions that possibly conflict with the simulation model results. First: the general trend of increasing the underload ratio leading to increased performance holds true. The fewer subcarriers with actual data, the less intersymbol interference. With greater underloading ratios, the farther apart the information symbols become in either the frequency or chirp domains, guarding them from each other similar to a guard band between transmit symbols.

Second, for an underload ratio of 1 (i.e. no underloading), OCDM dramatically outperforms OFDM as the number of subcarriers is increased. However, this is not necessarily the case in the 16 subcarrier signal set, nor is it necessarily the case as the underload ratio is increased: in both cases it would be expected that OCDM outperforms OFDM for all the tested signal permutations as per the simulation model.

Third, for the smaller numbers of subcarriers, it is not necessarily true that increasing the underload ratio (thereby reducing the number of subcarriers with useful information) actually results in an increase in performance. For the 64 subcarrier signal permutations, it could be argued that the reason for the error rates of 0, and the error rate of 4.1528e-4 for OCDM with an underload ratio of 8, could be caused

by a lack of signal resolution. Transmitting more symbols over a longer period of time may result in trends more similar to the 256 subcarrier signal sets.

In general there seems to be a sweetspot for performance: the 64 subcarrier signals outperformed both the 256 subcarrier signals and the 16 subcarrier signals. This could be because the signals with more subcarriers are more subject to errors in clock drift, while the signals with fewer subcarriers could be more subject to the effects of multipath causing more intersymbol interference. The 16 subcarrier signal set has relatively poor performance compared to the other two signal sets.

The 16 subcarrier signal set could also suffer from channel resolution problems. The channel is estimated for each subcarrier, and with only 16 subcarriers there may not be enough resolution to accurately recover the channel for the purposes of data recovery. This assumption is supported by [25]. The accuracy of the channel estimation has a large impact on OCDM in comparison to OFDM. [25] also points out that reducing the guard interval reduces the performance of OCDM. The signals transmitted in the Aquatron experiment have very very short guard intervals because of the previously mentioned issues with the function generator. The impact of the guard interval should be investigated in future works.

The gap in performance in the simulation as compared to the Aquatron experiment could also be explained by the differences in the channels. The St. Margaret's Bay channel (Figure 4.1) has much less multipath than the Aquatron channel (Figure 4.16). The simple equalizer used in the Aquatron experiment may not be sufficient to recover the data. The MMSE equalizer used in simulation is not used in the Aquatron experiment. An improved equalizer might improve performance.

Throughput achieved in the simulation and experiment demonstrates that both OFDM and OCDM can be implemented as much higher throughput underwater communication techniques. The simulation was able to achieve relatively strong performance at speeds as high as 905 bps. The Aquatron experiment achieved speeds as high as 2500 bps with reasonable performance.

This experiment does not address the covertness of OCDM. Future work should allow for an experiment with one transmitter and two receivers (an intended target and an interceptor) placed at various distances and transmitted at low power to determine how much of the signal can be recovered by an unintended interceptor.

Directional beamforming could be incorporated in to this proposed experiment to reduce signal energy outside of its intended path of arrival: this would necessitate pre-knowledge of the intended transmission target. A method for determining the location of an intended target covertly could also be investigated.

Chapter 5

Conclusion

In the modern era, more robust methods for secure, covert underwater wireless acoustic communication are necessary to protect the territorial waters that are changing due to melting sea ice caused by global warming. Current techniques are either reliable but low-throughput, or high-throughput but very susceptible to the underwater channel conditions.

In this work, OCDM has been proposed as a time modulation technique to provide a link that is both high-throughput and resilient to the effects of the underwater channel. After comparing it to OFDM, it can be said generally that OCDM mildly outperforms OFDM in the presence of multipath. It has also been demonstrated that the performance of OCDM appears to be heavily influenced by accurate channel estimation information. In fact, it is suspected that a low number of subcarriers does not provide enough resolution for channel estimation to allow for good performance. However, as the number of subcarriers increases, the improvement in reliability is significant compared to OFDM. For this experiment, an optimal number is 64 subcarriers: this may be due to the presence of the Doppler effect that was not well-compensated for during this experiment. The experiment is also constrained on the potential clock drift between the transmitter and receiver. Finally, in the Aquatron, the MMSE equalizer was not implemented with OCDM. The MMSE equalizer is integral to the excellent performance of OCDM in simulation, and should be included in future experiments.

At higher numbers of subcarriers, underloading can dramatically improve the performance of OCDM but does not have as much of an impact on the performance of OFDM. Channel estimation should be performed with a pilot symbol instead of one of the transmit data symbols to allow for a channel estimate using the full frequency range of the channel: when underloading, the transmit symbol is missing information about the frequency band (because OCDM spans the whole band, it has frequency

diversity). OFDM does not suffer from this frequency diversity problem. For both OFDM and OCDM, increasing bandwidth decreases performance. Bandwidth can be improved by performing pre-equalization at the transmitter to reduce the impact of the front-end frequency selective transducer response without a dramatic decrease in performance but with a reduction in signal level.

Finally, to use OCDM as a covert link, it should be combined with some form of spread spectrum technique (each chirp represents one piece of the code) [6]. Follow up research on covert communication links should include modeling and experimentation with one transmitter and 2 receivers (one acting as the intended recipient and one acting as unintended recipient) at different distances. Suggestions for continuing research focus on adding covertness with coding techniques and spread spectrum techniques, and the impact of spatial modulation techniques such as directional beamforming.

Bibliography

[1] GISS Surface Temperature Analysis (GISTEMP v4). https://data.giss.nasa.gov/gistemp/. Accessed: 2021-06-01.

[2] Arctic sea ice decline stalls out at second lowest minimum. https://nsidc.org/arcticseaicenews/2020/09/arctic-sea-ice-decline-stalls-out-at-second-lowest-minimum/. Accessed: 2021-06-01.

[3] Canada's Northwest Passage claim isn't settled — but it's not 'illegitimate,' like the U.S. says it is. https://globalnews.ca/news/5256532/northwest-passage-canada-us-claim-challenge/. Accessed: 2021-06-01.

[4] Y. Bernaldo de Quirós, A. Fernandez, R. W. Baird, R. L. Brownell, N. Aguilar de Soto, D. Allen, M. Arbelo, M. Arregui, A. Costidis, A. Fahlman, A. Frantzis, F. M. D. Gulland, M. Iñíguez, M. Johnson, A. Komnenou, H. Koopman, D. A. Pabst, W. D. Roe, E. Sierra, M. Tejedor, and G. Schorr. Advances in Research on the Impacts of Anti-submarine Sonar on Beaked Whales. *Proceedings of the Royal Society B: Biological Sciences*, 286(1895):20182533, 2019.

[5] JANUS, the CMRE underwater communication protocol, becomes a NATO Standard. https://www.cmre.nato.int/rockstories-blog-display/398-janus-the-cmre-underwater-communication-protocol-becomes-a-nato-standard#~:text=It-is-called-JANUS-and-it-has-been,way-for-a-standardised-Internet-of-Underwater-Things. Accessed: 2022-01-07.

[6] Emrecan Demirors and Tommaso Melodia. Chirp-Based LPD/LPI Underwater Acoustic Communications with Code-Time-Frequency Multidimensional Spreading. In *Procs. of the 11th ACM Intl. Conference on Underwater Networks '&' Systems*, WUWNet '16, New York, NY, USA, 2016. Association for Computing Machinery.

[7] R. Diamant and L. Lampe. Low Probability of Detection for Underwater Acoustic Communication: A Review. *IEEE Access*, 6:19099–19112, Apr. 2018.

[8] R. A. Scholtz M. L. Simon, K. K. Omura and B. K. Levitt. *Spread Spectrum Communications Handbook*. McGraw-Hill, 1994.

[9] W. L. Hopkins N. C. Beaulieu and P. J. McLane. Interception of frequency-hopped spread-spectrum signals. *IEEE J. Sel. Areas Commun.*, 8(5):853–870, Jun. 1990.

[10] A. Pescetto M. Palmese, G. Bertolotto and A. Trucco. Experimental validation of a chirp-based underwater acoustic communication method. *Proc. Meetings Acoust.*, 4(1):030002, 2008.

[11] Julian F.V Vincent, Olga A Bogatyreva, Nikolaj R Bogatyrev, Adrian Bowyer, and Anja-Karina Pahl. Biomimetics: its Practice and Theory. *Journal of The Royal Society Interface*, 3(9):471–482, 2006.

[12] Jongmin Ahn et al 2019. Mimicking Dolphin Whistles with Continuously Carying Carrier Frequency Modulation for Covert Underwater Acoustic Communication. *Jpn. J. Appl. Phys.*, 58(SGGF05), 2019.

[13] Gang Qiao Songzuo Liu and Asim Ismail. Covert Underwater Acoustic Communication using Dolphin Sounds. *The Journal of the Acoustical Society of America*, 113, 2013.

[14] M. Stojanovic, J.G. Proakis, J.A. Rice, and M.D. Green. Spread Spectrum Underwater Acoustic Telemetry. In *IEEE Oceanic Engineering Society. OCEANS'98. Conference Proceedings*, volume 2, pages 650–654 vol.2, 1998.

[15] J. Potter, J. Alves, D. Green, G. Zappa, I. Nissen, and K. McCoy. The JANUS underwater communications standard. In *2014 Underwater Communications and Networking (UComms)*, pages 1–4, 2014.

[16] Jinfeng Li, Joseph Halt, and Y. Rosa Zheng. Utilizing JANUS for Very High Frequency Underwater Acoustic Modem. In *Global Oceans 2020: Singapore – U.S. Gulf Coast*, pages 1–6, 2020.

[17] R. Nabar A. Paulraj and D. Gore. *Introduction to Space-Time Wireless Communications*. Cambridge University Press, 2003.

[18] Baojian Gao, Zhenzhen Fan, Xingyuan Liu, Lihua Zhang, and Xiwen Ouyang. OFDM Covert Communication System Based on the QC-LDPC and Symbol Spread Spectrum. In *2020 Cross Strait Radio Science & Wireless Technology Conference (CSRSWTC)*, pages 1–3, 2020.

[19] C. Schlegel et al. UMDCC Report 2015-2016, 2016.

[20] Ali M. Bassam. OFDM Transmission for Doubly Dispersive Underwater Acoustic Channels. Master's thesis, Dalhousie University, The address of the publisher, 3 2015.

[21] Xing Ouyang and Jian Zhao. Orthogonal Chirp Division Multiplexing for Coherent Optical Fiber Communications. *Journal of Lightwave Technology*, 34(18):4376–4386, 2016.

[22] Yiqi Bai and Pierre-Jean Bouvet. Orthogonal Chirp Division Multiplexing for Underwater Acoustic Communication. *Sensors*, 18(11), 2018.

[23] Xing Ouyang, Cleitus Antony, Fatima Gunning, Hongyu Zhang, and Yong Liang Guan. Discrete Fresnel Transform and Its Circular Convolution, 2015.

[24] Xiaohua Li and H. Fan. Direct estimation of blind zero-forcing equalizers based on second-order statistics. *IEEE Transactions on Signal Processing*, 48(8):2211–2218, 2000.

[25] T. P. Sameer Babu, Jobin Francis, and R. David Koilpillai. OTFS and OCDM Based Underwater Acoustic Communication: System Design and Evaluation. In *OCEANS 2022, Hampton Roads*, pages 1–6, 2022.